

LRRK2 AND THE p.G2019S MUTATION IN NEURONAL AND SYSTEMIC RESPONSE
TO INDUCED α -SYNUCLEIN PATHOBIOLOGY

by

Sarah MacIsaac

H.B.Sc., The University of Toronto, 2014

A THESIS SUBMITTED IN PARTIAL FULFILLMENT OF
THE REQUIREMENTS FOR THE DEGREE OF

MASTER OF SCIENCE

in

THE FACULTY OF GRADUATE AND POSTDOCTORAL STUDIES
(Neuroscience)

THE UNIVERSITY OF BRITISH COLUMBIA
(Vancouver)

July 2016

© Sarah MacIsaac, 2016

Abstract

Parkinson's disease (PD) is a progressive neurodegenerative disorder for which no disease-modifying treatments are currently available. PD is neuropathologically characterized by selective degeneration of nigral dopaminergic neurons and the presence of intraneuronal inclusions comprised primarily of α -synuclein (α -syn) in remaining cells. Mutations in several genes have been linked to PD, including those encoding α -syn and leucine-rich repeat kinase 2 (LRRK2). α -Syn pathology is present in the majority of patients with LRRK2 mutations, and a synergistic pathology has been proposed. A model of α -synucleinopathy was recently developed in which pathogenic α -syn pre-formed fibrils (PFFs) are used to seed aggregation of endogenous α -syn. To probe the role of LRRK2 and the influence of the p.G2019S mutation in induced α -syn pathology, differences in the response of wild-type (WT), LRRK2 knock-out (KO), and p.G2019S LRRK2 knock-in (KI) primary neuronal cultures to PFF treatment were examined. Further, behavioural consequences of intrastriatal PFF injection in WT and p.G2019S LRRK2 KI mice were compared. LRRK2 KO cultures appeared to be protected from PFF treatment, possibly due to a reduction in PFF uptake, more efficient degradation of pathogenic α -syn in neurites, and/or less neuron-to-neuron spread of pathogenic α -syn. Alternatively, p.G2019S LRRK2 KI cultures appeared to be more susceptible to PFF treatment, perhaps due to impaired handling of pathogenic α -syn by after fibril uptake. Behaviourally, WT and p.G2019S LRRK2 KI mice appear similarly vulnerable to motor deficits, but p.G2019S LRRK2 KI mice may be more susceptible to PFF-induced anxiety and cognitive deficits. Overall, this research points towards multiple roles for LRRK2 in α -syn pathogenic processes that may be altered by the p.G2019S mutation.

Preface

The following research was conducted at the Centre for Applied Neurogenetics under the supervision of Dr. Austen Milnerwood and Dr. Matthew Farrer. All experiments and analyses were performed by Sarah MacIsaac with assistance from Dr. Mattia Volta for *in vivo* experimental design, Dr. Catherine Cowan for electron microscopy, Alina Maschirow for behavioural testing, and Michael Smythies for image acquisition, image processing, and cylinder test scoring. This manuscript was written by Sarah MacIsaac and edited by Dr. Milnerwood. All experiments were conducted in accordance with the Canadian Council on Animal Care, with approval by the Animal Care Committee at the University of British Columbia under protocol numbers A15-0105 and A16-0088.

Table of Contents

Abstract.....	ii
Preface.....	iii
Table of Contents	iv
List of Figures.....	vii
List of Abbreviations	viii
Acknowledgements	xii
1. Introduction.....	1
1.1 Parkinson’s disease	1
1.2 The genetics of Parkinson’s disease	2
1.2.1 <i>SNCA</i> mutations	3
1.2.1.1 The α -synuclein protein.....	4
1.2.1.2 Modeling <i>SNCA</i> mutations	5
1.2.2 <i>LRRK2</i> mutations	6
1.2.2.1 The leucine-rich repeat kinase 2 protein.....	7
1.2.2.2 Modeling <i>LRRK2</i> mutations.....	8
1.3 α -Synuclein and leucine-rich repeat kinase 2.....	10
1.4 α -Synucleinopathies	11
1.4.1 Progression of α -synuclein pathology	12
1.4.2 The pathological α -synuclein protein.....	13
1.4.3 Modeling α -synuclein pathology.....	14
1.5 Rationale for present experiments	16

2. Methods.....	18
2.1 Subjects.....	18
2.2 Primary neuronal culture and nucleofection.....	18
2.3 Electron microscopy.....	19
2.4 Culture pre-formed fibril treatments.....	19
2.5 Lactate dehydrogenase assay.....	20
2.6 Immunocytochemistry.....	20
2.7 Fluorescence imaging and analysis.....	21
2.8 Behavioural testing.....	22
2.8.1 Apparatus.....	22
2.8.2 Testing paradigms.....	23
2.8.3 Scoring and analysis.....	24
2.9 Stereotaxic surgery.....	24
2.10 Statistics.....	25
3. Results.....	26
3.1 Induced α -synucleinopathy in primary neurons by pre-formed fibril treatment.....	26
3.1.1 Monomeric α -synuclein does not induce α -synucleinopathy.....	26
3.1.2 Leucine-rich repeat kinase 2 knock-out neurons are protected from pre-formed fibril-induced α -synucleinopathy.....	26
3.1.3 p.G2019S leucine-rich repeat kinase 2 knock-in neurons are more susceptible to pre-formed fibril treatment-induced α -synucleinopathy.....	32
3.2 Induced behavioural deficits in mice by intrastriatal pre-formed fibril injection.....	37

3.2.3 p.G2019S leucine-rich repeat kinase 2 knock-in mice may be more susceptible to pre-formed fibril-induced cognitive deficits	42
4. Discussion	45
4.1 Initial characterization of pre-formed fibril treatment	45
4.2 The role of leucine-rich repeat kinase 2 in neuronal response to induced α -synucleinopathy by pre-formed fibril treatment	47
4.3 p.G2019S-induced alterations in neuronal response to induced α -synucleinopathy by pre-formed fibril treatment	51
4.4 p.G2019S-induced alterations in behavioural deficits caused by intrastriatal pre-formed fibril injection.....	53
4.5 Limitations and future directions	57
4.5.1 Markers of α -synucleinopathy <i>in vitro</i>	57
4.5.2 Mechanisms of genotypic differences <i>in vitro</i>	57
4.5.3 Immunohistochemistry staining <i>in vivo</i>	58
5. Conclusion	59
Bibliography	60

List of Figures

Figure 1. Transmission electron microscopy of α -synuclein pre-formed fibrils pre- and post-sonication.	27
Figure 2. Treatment with α -synuclein monomer does not induce α -synucleinopathy.	28
Figure 3. Basic characterization of pre-formed fibril treatment in primary neurons.	29
Figure 4. Pre-formed fibril treatment of leucine-rich repeat kinase 2 knock-out primary neurons.	30
Figure 5. The autophagy marker p62 in pre-formed fibril-treated leucine-rich repeat kinase 2 knock-out primary neurons.	31
Figure 6. The lysosomal marker LAMP1 in pre-formed fibril-treated leucine-rich repeat kinase 2 knock-out primary neurons.	33
Figure 7. Pre-formed fibril treatment of leucine-rich repeat kinase 2 p.G2019S knock-in primary neurons.	34
Figure 8. The autophagy marker p62 in pre-formed fibril-treated leucine-rich repeat kinase 2 p.G2019S knock-in primary neurons.	36
Figure 9. Injection site of α -synuclein pre-formed fibrils.	38
Figure 10. Motor testing of pre-formed fibril-injected leucine-rich repeat kinase 2 p.G2019S knock-in mice.	39
Figure 11. Anxiety testing of pre-formed fibril-injected leucine-rich repeat kinase 2 p.G2019S knock-in mice.	41
Figure 12. Cognitive testing of pre-formed fibril-injected leucine-rich repeat kinase 2 p.G2019S knock-in mice using the novel object location test.	43
Figure 13. Cognitive testing of pre-formed fibril-injected leucine-rich repeat kinase 2 p.G2019S knock-in mice using the puzzle box test.	44

List of Abbreviations

λ_{\max} : wavelength of maximum absorbance

81A: antibody for α -synuclein phosphorylated at serine 129

ACB: affected cell body

ANOVA: analysis of variance

AP: anterior/posterior

ASO: antisense oligonucleotide

α -Syn: α -synuclein protein

Ca^{2+} : calcium ions

cm: centimetres

CMA: chaperone-mediated autophagy

CPR: centre path ratio

DA: dopamine

DAPI: 4',6-diamidino-2-phenylindole

DIV: days in vitro

DV: dorsal/ventral

E: embryonic day

EDTA: ethylenediaminetetraacetic acid

ERK: extracellular signal-related kinase

g: grams

GFAP: glial fibrillary acidic protein

GFP: green fluorescent protein

GTPase: guanine triphosphate hydrolase enzyme

GWAS: genome wide association studies

h: hours

HA-tag: human influenza hemagglutinin amino acids 98-106 epitope tag

HBSS: Hank's Balanced Salt Solution

Hepes: 4-(2-hydroxyethyl)-1-piperazineethanesulfonic acid

Het: heterozygous for the LRRK2 p.G2019S mutation

Homo: homozygous for the LRRK2 p.G2019S mutation

Iba1: ionized calcium-binding adaptor molecule 1

KI: leucine-rich repeat kinase 2 p.G2019S knock-in

KO: leucine-rich repeat kinase 2 knock-out

l: litres

L: length

LAMP1: lysosomal-associated membrane protein 1

LBs: Lewy bodies

LDH: lactate dehydrogenase

LN: Lewy neurites

LRRK2: leucine-rich repeat kinase 2

M83: transgenic mice overexpressing p.A53T α -synuclein under the murine prion promoter

μ g: micrograms

μ l: microliters

μ m: micrometres

m: metres

MAP2: microtubule-associated protein 2

mo: months

min: minutes

ml: millilitres

ML: medial/lateral

mM: millimolar

mRNA: messenger ribonucleic acid

NAC: non-beta-amyloid component

NAD⁺: oxidized nicotinamide adenine dinucleotide

NADH: reduced nicotinamide adenine dinucleotide

NGS: normal goat serum

nm: nanometres

NOL: novel object location behavioural paradigm

p62: sequestosome-1

PBS: phosphate-buffered saline

PBST: phosphate-buffered saline with 0.02% Tween-20

PCR: polymerase chain reaction

PD: Parkinson's disease

PFA: paraformaldehyde

PFFs: pre-formed fibrils of α -synuclein

PKG: phosphoglycerate kinase I promoter

p-Syn: α -synuclein protein phosphorylated at residue serine 129

ROI: region of interest

s: seconds

Ser129: residue serine 129

SNCA: α -synuclein gene

SNARE: soluble *N*-ethylmaleimide-sensitive factor attachment protein receptor

SNC: substantia nigra pars compacta

TEM: transmission electron microscope

Tx: trial x

TH: tyrosine hydroxylase

W: width

WT: wild-type

Acknowledgements

I am so appreciative to everyone in this lab for their professional and personal support during my time here. I am especially grateful to Austen for encouraging constant questioning and doubt for the sake of scientific accuracy while still embracing an optimistic outlook. I am indebted to Jas for being such an invaluable resource of technical knowledge, and to Stefano for being a dual punching bag-cuddle buddy amid data disasters. I very much appreciate the contributions of everybody who was involved in this project either directly or peripherally at any stage, especially Daisy, Stefano, Jesse, Alina, Michael, Silvia, and Jas. Finally, I would like to thank all of the wonderful people in my life outside of the lab who have supported me throughout this endeavour.

1. Introduction

1.1 Parkinson's disease

First described by James Parkinson in 1817 in 'An Essay on the Shaking Palsy' (Parkinson, 1817), Parkinson's disease (PD) is a progressive neurodegenerative disorder that affects up to 2% of people over age 80 (Pringsheim et al., 2014). It has been traditionally characterized as a movement disorder, and is clinically diagnosed after the presentation of motor symptoms including rigidity, tremor, bradykinesia, and postural instability. However, PD is also accompanied by non-motor symptoms that can present decades before the onset of motor symptoms; these include hyposmia, autonomic dysfunction, sleep disturbances, and mood disorders (Stern et al., 2012; Berg et al., 2015). Although the majority of PD cases are idiopathic, several genetic mutations have been linked to familial parkinsonism and/or associated with risk for sporadic PD.

Neuropathologically, PD is characterized post-mortem by a) selective degeneration of dopaminergic neurons of the substantia nigra pars compacta (SNc) that project to the striatum, and b) the presence of Lewy bodies (LBs) and neurites (LNs), intraneuronal inclusions comprised primarily of α -synuclein (α -syn), in the soma and processes of surviving neurons (Dickson, 2012). These inclusions are present throughout the brainstem and midbrain, and more sparsely in cortical and limbic regions (Arnold et al., 2013).

No common disease mechanism has been elucidated for sporadic or familial parkinsonism as of yet. Dopamine (DA) replacement therapy (levodopa) is the most common therapeutic strategy and can provide temporary relief from cardinal motor symptoms; however, it does not have sustaining positive effects, often causes dyskinesia, and does nothing to address debilitating non-motor symptoms (Smith et al., 2012). Currently, no therapeutic agents slow disease progression or prevent onset.

1.2 The genetics of Parkinson's disease

The discovery of mutations linked to familial parkinsonism and genetic variability associated with sporadic PD risk has recently begun to provide some understanding of disease etiology. Firstly, longitudinal observation of individuals carrying mutations linked to familial PD has led to the discovery of predictive clinical traits that can present several years before motor symptom onset, such as rapid eye movement sleep behaviour disorder, olfactory loss, constipation, and/or hypotension (Berg et al., 2015). These traits implicate a subtle disease process that may develop over decades, hinting at the possibility of early interventions for familial and idiopathic PD that could slow or halt progression. Furthermore, *in vitro* and *in vivo* studies of normal and mutant functions of relevant proteins have suggested alterations to vesicular dynamics and synaptic function are central to PD pathogenesis, bringing the field closer to a mechanistic understanding of the disease and the ability to design novel therapeutic approaches (Volta et al., 2015b). Finally, uncovering causal mutations has led to the development of animal models expressing mutant proteins, enabling long-term studies that characterize the temporal neurobiological consequences of their expression. As of yet, no transgenic model of PD has replicated all cardinal features of the disease, likely due to intrinsic differences between rodents and humans as well as the relatively short lifespans of model systems. However, this avenue of study has the potential to reveal early and subtle changes caused by these mutations, to identify predictive biomarkers for late-stage disease, and to test efficacy of therapeutic agents aimed at neuroprotection for PD and related diseases.

1.2.1 *SNCA* mutations

The first genetic link to PD was discovered in 1997 by Polymeropoulos et al., who found the p.A53T missense mutation of the gene encoding α -syn (*SNCA*) was linked to early-onset familial parkinsonism in an Italian family (Polymeropoulos et al., 1997). Subsequent studies have identified the p.A30P, p.E46K, p.H50Q, and p.G51D missense mutations in the *SNCA* locus are also linked to autosomal-dominant PD (Lin and Farrer, 2014). These patients appear clinically and histopathologically indistinguishable from patients with idiopathic PD, displaying levodopa-responsive parkinsonism with diffuse Lewy pathology (Trinh and Farrer, 2013).

Multiplication mutations in *SNCA* that increase α -syn load have also been linked to familial PD, suggesting that increased α -syn protein levels are sufficient to cause disease (Singleton et al., 2003; Miller et al., 2004). These patients also display levodopa-responsive parkinsonism, but with greater instance of autonomic dysfunction, cognitive decline, and dementia (Nishioka et al., 2009). Interestingly, *SNCA* multiplication mutations display dose-dependency, where triplication is associated with earlier disease onset and faster disease progression than duplication (Fuchs et al., 2007). α -Syn multiplication results in diffuse Lewy pathology with both nigral and hippocampal CA2-3 neuronal loss (Trinh and Farrer, 2013).

Finally, genome wide association studies (GWAS) have highlighted several polymorphisms that contribute to sporadic PD risk; in fact, variability in the *SNCA* locus confers the highest risk for idiopathic PD (Nalls et al., 2014). *SNCA* is one of only two genes both linked to familial PD and associated with sporadic PD. Mutations in the *SNCA* gene are also of particular interest given that α -syn is the primary component of Lewy inclusions, one of the defining histopathological features of PD.

1.2.1.1 The α -synuclein protein

Unfortunately, the field only has a vague understanding of the normal function of α -syn and how genetic changes linked to/associated with PD affect its structure and function. The 140-amino acid protein has a lipid-binding N-terminal region (residues 1-60), a central hydrophobic NAC region (61-95) that confers the protein's propensity to form β -sheets and that is necessary for α -syn aggregation, and a negatively charged C-terminal region (96-140). It has a natively unfolded structure in aqueous solution, but may associate with other α -syn proteins in a tetramer conformation upon lipid binding (Bartels et al., 2011). Highly expressed throughout the brain, α -syn preferentially localizes to presynaptic terminals and is thought to contribute to membrane curvature (Westphal and Chandra, 2013), SNARE complex formation (Burré et al., 2010), and vesicle storage and recycling (Nemani et al., 2010; Südhof et al., 2011).

There is little consensus with regards to the functional significance of α -syn mutations, although gene-dose dependency of *SNCA* suggests gain-of-function toxicity. All linked missense mutations reside in the lipid-binding motif of α -syn, but do not seem to influence lipid-binding capabilities. The two leading theories of pathogenic processes initiated by α -syn mutations are 1) alterations at the synapse resulting in excess Ca^{2+} influx or neurotransmitter leakage through membrane pore formation (Danzer et al., 2007; Mosharov et al., 2009), and 2) induced impairments in protein degradation and sorting systems, resulting in disrupted cellular homeostasis (Martinez-Vicente and Vila, 2013). The p.A53T and p.A30P mutations increase the rate of α -syn oligomer formation, which is toxic to neurons (Conway et al., 2000). This may be due to the disruption of membrane integrity (Volles and Lansbury, 2002), an aberrant influence on proteasomes or lysosomes impairing protein degradation (Xilouri et al., 2009; Emmanouilidou et al., 2010), and/or seeding aggregation and spreading of non-toxic α -syn (Wood et al., 1999;

Peelaerts et al., 2015). However, the p.E46K mutation actually reduces the rate of α -syn oligomer formation relative to the WT protein (Fredenburg et al., 2007); therefore, this theory does not explain the negative effects of all PD-linked α -syn missense mutations. Regarding duplication and triplication mutations, overexpression (OE) of WT α -syn is generally considered to be analogous to *SNCA* multiplication and has also been observed to increase neuronal susceptibility to insult, likely also by disrupting synaptic function (Garcia-Reitböck et al., 2010) and imposing undue stress on protein degradation pathways (Anandhan et al., 2015).

1.2.1.2 Modeling SNCA mutations

Many transgenic rodent models have been developed based on α -syn missense and multiplication mutations, and have generally relied on OE of WT, p.A30P, and/or p.A53T α -syn under various promoters. Most of these models only partially recapitulate the key features of disease and often do not involve dopaminergic dysfunction (Chesselet and Richter, 2011). Further, while OE of the WT protein may mimic the effects of α -syn gene multiplication in humans, overexpressing mutant variants confounds interpretation of induced consequences that cannot be specifically attributed to the mutation or OE. Nigral cell death, depletion of nigrostriatal dopamine markers, and α -syn aggregation are not typically observed together in any single mouse model, and are generally limited to models that overexpress very high levels of mutant α -syn (Chesselet and Richter, 2011). Further, while virtually all genetic α -syn models display a motor phenotype, only some have been shown to exhibit non-motor behavioural alterations such as sensory, autonomic, cognitive or anxiety phenotypes (Chesselet and Richter, 2011).

Most rat models of genetic PD focus on viral-driven expression of WT or mutant α -syn in the nigra, likely due to the fact that genomic editing, breeding, and maintenance of rat colonies is

comparatively more difficult, time consuming, and costly (Welchko et al., 2012; Volpicelli-Daley et al., 2016b). Though many of these models produce rapid, robust nigral cell death and α -syn pathology, as soon as 3 weeks post-injection (Kirik et al., 2002; Lo Bianco et al., 2002; Yamada et al., 2004; Koprach et al., 2011), this somewhat severe approach is not amenable to understanding early or progressive disease processes.

In summary, although mutations in the *SNCA* gene have provided important clues regarding the etiology of PD, our understanding of how altered α -syn levels and mutations result in disease pathogenesis is limited.

1.2.2 *LRRK2* mutations

Mutations in the *LRRK2* gene, which encodes the leucine-rich repeat kinase 2 (LRRK2) protein, were first linked to dominantly inherited parkinsonism in 2004 (Paisán-Ruiz et al., 2004; Zimprich et al., 2004). Shortly after, the LRRK2 p.G2019S mutation was found in several European families (Kachergus et al., 2005), and identified as the primary cause of assumed sporadic PD in Ashkenazi Jews, Norwegians, and North-African Berbers (Clark et al., 2006; Ozelius et al., 2006; Hentati et al., 2014). The p.G2019S mutation is now known to be the most common cause of genetic Parkinson's disease worldwide, assumed to be responsible for 1-2% of familial and sporadic PD (Lin and Farrer, 2014). Linkage analyses have similarly identified several other PD-causing LRRK2 mutations, including p.R1437H, p.R1441H/G/C, p.Y1699C, and p.12020T (Lin and Farrer, 2014). LRRK2 parkinsonism appears clinically indistinguishable from sporadic PD, but post-mortem analyses have revealed heterogeneity in pathological features. Though most individuals have diffuse LB pathology (Ross et al., 2006), others present with tauopathy, TDP43 and ubiquitin-positive aggregates, or nigral degeneration without aggregate

pathology, likely reflecting the presence of environmental or genetic modifiers (Zimprich et al., 2004; Rajput et al., 2006). Furthermore, pleomorphic pathology within LRRK2 parkinsonism suggests LRRK2 dysfunction must be upstream and independent of resultant pathological aggregation.

Genetic variability in the *LRRK2* locus has also been associated with risk of idiopathic PD by GWAS, making it the second gene (along with *SNCA*) both linked to familial PD and associated with sporadic PD.

1.2.2.1 The leucine-rich repeat kinase 2 protein

The physiological role of the LRRK2 protein is poorly understood. LRRK2 is a large ~280 kDa protein that is ubiquitously expressed and has many functional capabilities; the protein has GTPase and kinase domains among other functional regions, and regulates its GTPase activity via autophosphorylation. Neuronal consequences of *in vitro* LRRK2 knock-out (KO)/knock-down (KD) studies have pointed towards roles for LRRK2 in regulation of synaptic vesicle trafficking at the presynapse (Piccoli et al., 2011) and cytoskeletal dynamics (MacLeod et al., 2006; Parisiadou et al., 2009; Häbig et al., 2013). However, the size of LRRK2 has made it an extremely difficult protein to study *in vitro*; development of reliable antibodies has been challenging (Davies et al., 2013), and thus there has been little insight into its subcellular localization and protein-protein interactions until recently. Schreij et al. engineered a cell line expressing HA-tagged LRRK2 and showed that the protein predominantly localizes to endosomes and interacts with clathrin-light chains, an interesting finding in light of the field's current mechanistic understanding of PD (Schreij et al., 2015). Recent phosphoproteomics work has also pointed to members of the Rab-GTPase protein family as downstream phosphorylation targets for LRRK2 (Steger et al., 2016).

Rab-GTPases are known to be intimately involved in the regulation of vesicular dynamics, including pathways responsible for protein sorting/degradation and synaptic transmission.

Most PD-related LRRK2 mutations lie within the GTPase or kinase domains of the protein. The gain-of-function p.G2019S mutation is located within the kinase domain and increases the protein's kinase activity by at least three-fold, altering its autophosphorylation and substrate phosphorylation activity (West et al., 2005). In light of this, many groups have recently focused on development of LRRK2 kinase inhibitors (Leveridge et al., 2016) or antisense oligonucleotides (ASOs) (Volta et al., 2015a) targeting mRNA for therapeutic purposes. The mutation has been observed to cause neuronal abnormalities *in vitro* including neurite abnormalities, Ca²⁺ dysfunction, and synaptic alterations (Lin et al., 2010; Beccano-Kelly et al., 2014; Schwab and Ebert, 2015). In addition, the p.G2019S mutation has been observed to augment autophagy (Su and Qi, 2013), an intracellular protein degradation mechanism in which waste is targeted and delivered to lysosomes for breakdown. However, no clear mechanism with regards to how the p.G2019S mutation specifically causes downstream dysfunction has been elucidated.

1.2.2.2 Modeling LRRK2 mutations

There are fewer genetic rodent models of PD based on *LRRK2* than *SNCA*, reflecting the fact that *SNCA* was linked to PD six years prior to *LRRK2*. Several groups, including ours, have examined bacterial artificial chromosome (BAC) OE or tetracycline-controlled expression of human WT, p.G2019S, or p.R1441G/C LRRK2 in mice and rats (Melrose et al., 2010; Sloan et al., 2012, 2016; Xu et al., 2012; Beccano-Kelly et al., 2014, 2015; Volta et al., 2015a). Many of these lines do not display a motor phenotype or nigral loss, though some show altered striatal dopamine neurotransmission with age (Lin et al., 2009; Li et al., 2010; Melrose et al., 2010).

There are many inherent caveats to BAC OE, including random gene insertion, variable expression patterns, parallel exogenous and endogenous expression, and inability to interpret if effects are mutation-specific. Thus, a LRRK2 p.G2019S knock-in (KI) mouse line was developed by Dr. Matthew Farrer at the Mayo Clinic by insertion of a floxed PGK-neomycin cassette between *LRRK2* exons 41 and 42. LRRK2 p.G2019S KI mice express endogenous levels of mutant LRRK2 and thus inevitable OE confounds are eliminated. Mice from the LRRK2 p.G2019S KI line do not develop cardinal PD histopathological end-points (i.e. nigral cell loss and α -syn aggregation), likely due to their relatively short life span. However, the model shows great promise for studying early changes that this subtle genetic alteration induces in patients. KI effects have been partially characterized *in vitro* and *in vivo*; physiologically, LRRK2 p.G2019S KI primary cortical neurons have an increased probability of glutamate release (Beccano-Kelly et al., 2014) and mice have reduced basal and drug-evoked extracellular dopamine in the striatum (Yue et al., 2015). As glutamatergic inputs from the cortex and dopaminergic inputs from the nigra converge at the striatum, these data suggest that altered vesicular dynamics and synaptic dysfunction in the striatum are early changes caused by the p.G2019S mutation. Reflecting these changes at the behavioural level, LRRK2 p.G2019S KI mice were observed to be hyperactive and resistant to age-related hypoactivity beginning after six months of age, an effect eliminated by LRRK2 kinase inhibition (Longo et al., 2014). Our own group has also observed subtle hyperactivity in LRRK2 p.G2019S KI mice that normalizes to WT levels around six months of age (unpublished data).

Discoveries regarding *LRRK2* mutations have been critical in advancing the field's understanding of PD, but a more in-depth characterization of its normal role as well as the cellular and systemic consequences of PD-causing *LRRK2* mutations is still very much needed in order to develop disease modifying therapies.

1.3 α -Synuclein and leucine-rich repeat kinase 2

The genetic linkage between α -syn, LRRK2, and PD is unequivocal. Several reports have suggested a synergistic pathological process between α -syn and LRRK2; unfortunately, there is a lack of consensus in the current literature. In 2009, LRRK2 was suggested to directly phosphorylate α -syn at residue serine 129 (Ser129) (Qing et al., 2009), an extremely intriguing finding in light of the knowledge that a) the p.G2019S mutation increases LRRK2 kinase activity, and b) α -syn is typically phosphorylated at this residue in Lewy inclusions (Fujiwara et al., 2002). However, this finding is considered controversial as it could not be replicated by other groups. OE of LRRK2 in cells has been reported to induce expression of α -syn through the extracellular signal-related kinase (ERK) pathway; however, the observed effect is modest and the p.G2019S mutation does not cause further pathway activation, suggesting this may not be a primary causal mechanism (Carballo-Carbajal et al., 2010). A direct interaction between α -syn and LRRK2 was more recently observed by immunofluorescence and co-immunoprecipitation (Guerreiro et al., 2013), although these findings also must be viewed through a critical lens given the non-specificity of many LRRK2 antibodies. Interestingly, this group also observed that LRRK2 KO cells show altered response to inducible α -syn pathology, suggesting LRRK2 may play a role in α -syn aggregate formation (Guerreiro et al., 2013).

The notion that LRRK2 is involved in response to pathogenic α -syn processes has been supported by several papers. p.A53T α -syn OE mice that are null for LRRK2 have been reported to show reduced pathology, neurodegeneration, and immune response relative to p.A53T α -syn OE mice with normal LRRK2 expression (Lin et al., 2009; Daher et al., 2012). In addition, LRRK2 KO rats and WT rats administered LRRK2 kinase inhibitors are protected from virally-expressed α -syn-mediated inflammation and nigral degeneration (Daher et al., 2014, 2015). With regards to

the specific influence of the LRRK2 p.G2019S mutation, OE of p.A53T α -syn with p.G2019S LRRK2 has been reported to exacerbate immune response and to non-significantly increase neurodegeneration relative to OE of p.A53T α -syn with WT LRRK2 (Lin et al., 2009). Further, OE of p.G2019S LRRK2 may exacerbate inducible α -syn pathology *in vitro* (Volpicelli-Daley et al. 2016, *in press*). Though intriguing, OE and viral expression have inherent caveats as previously discussed; thus, these findings require confirmation using more physiologically relevant methods. Investigation into the underlying mechanisms behind protection or vulnerability is also required.

1.4 α -Synucleinopathies

Interest in pathogenic α -syn lies not only in PD, but also in related disorders termed α -synucleinopathies. Similar inclusions have been found in these disorders including Parkinson's disease with dementia (PDD), dementia with Lewy bodies (DLB), and multiple system atrophy (MSA). The clinical and histopathological features of PDD and DLB are nearly identical to PD, but dementia presents as a key symptom after one year of PD diagnosis in the case of PDD or within one year in the case of DLB. Both PDD and DLB individuals tend to have greater Lewy pathology in cortical regions post-mortem. In MSA, clinical symptoms are severe, progress rapidly, and prominently feature autonomic dysfunction. MSA pathology also differs from other α -synucleinopathies: α -syn aggregates form in oligodendrocytes rather than neurons, and are present in relatively greater quantities within the cerebellum, midbrain, and cortex; and oligodendroglial death is observed in addition to neuronal death in the nigra. While these primary α -synucleinopathies show slight heterogeneity in presentation, there is much overlap between them in both clinical and histopathological features, suggesting a common underlying disease mechanism.

1.4.1 Progression of α -synuclein pathology

α -Syn pathology has been proposed to ascend in a progressive manner from the olfactory bulb and dorsal vagal nucleus to the midbrain and eventually the cortex (Braak et al., 2003). The legitimacy of ‘Braak staging’ is debated; the initial report’s methodology has been criticized for small sample sizes (Burke et al., 2008) and others have reported no correlation between LB pathology and clinical symptoms as assumed in the development of the staging scheme (Parkkinen et al., 2005). In fact, Lewy pathology has been discovered in post-mortem brains of healthy individuals (Parkkinen et al., 2005), and not all patients who display clinical signs of PD or Parkinson-like disorders show α -syn pathology post-mortem (Zimprich et al., 2004). The trend does appear to be valid in a large portion of Lewy pathology cases (Dickson et al., 2010), but its predictive ability and thus clinical utility is not entirely reliable.

However, a clinical study testing the efficacy of fetal graft transplantation to the striatum of PD patients initiated an important vein of research into α -syn pathology progression that is consistent with the notion of Braak staging. The brain of an individual who died several years after receiving a transplant was found to have α -syn pathology in grafted neurons, suggesting either direct transmission of α -syn species from host to graft or induced pathology due to external factors (Kordower et al., 2008). It was later shown using OE of myc-tagged α -syn that α -syn can be directly transmitted from cell-to cell via endocytic pathways, promoting inclusion formation (Desplats et al., 2009). Together, this clinical and experimental evidence informed a prionogenic hypothesis of α -syn (Olanow and Prusiner, 2009). According to this theory, pathogenic conditions induce the ‘misfolding’ of soluble α -syn into higher order, β -sheet rich oligomers and fibrils that go on to form aggregates. This toxic, misfolded α -syn can be transmitted between cells and seed the aggregation of non-toxic α -syn, causing a downstream cascade of pathology (Irwin et al.,

2013). More recent evidence that intracerebral injection of brain homogenate from symptomatic transgenic mice expressing the p.A53T mutation (M83 line) into young, asymptomatic M83 mice can accelerate development of α -syn pathology and symptom onset lent additional support to this hypothesis (Luk et al., 2012b).

1.4.2 The pathological α -synuclein protein

The exact nature of the toxic ‘species’ of α -syn has been hotly debated. It has been known for over 15 years that α -syn associates into higher order oligomers and fibrils in a nucleation-dependent process (Wood et al., 1999); however, if α -syn oligomers, fibrils, and/or aggregates cause or result from toxicity is still unclear. The consensus seems to point towards oligomers as the relevant toxic species in α -synucleinopathies: as previously mentioned, the *SNCA* p.A30P and p.A53T mutations both increase the rate of oligomer formation (Conway et al., 2000), and presence of oligomers is generally observed to correlate best with neurotoxicity (Gosavi et al., 2002). Indeed, α -syn variants that promote oligomer formation cause reduced mitochondrial activity and survival *in vitro* relative to variants with normal aggregation potential (Karpinar et al., 2009). Oligomer-forming variants also cause greater loss of nigral neurons when virally expressed *in vivo* relative to variants that promote fibril formation (Winner et al., 2011). Finally, DA and its metabolites have been suggested to inhibit conversion of proto-fibrillar species of α -syn to mature fibrils (Mazzulli et al., 2006). As DA and DA metabolites are present in high quantities in the SNc, the ratio of oligomeric to fibrillar α -syn may be increased in nigral neurons; if oligomers are toxic, the selective vulnerability of this region to degeneration in α -synucleinopathies may be explained.

1.4.3 Modeling α -synuclein pathology

Many attempts have been made to model α -syn pathology in rodents using transgenic approaches. As previously discussed, overexpressing α -syn often does not induce α -syn pathology, or does induce pathology that cannot be specifically attributable to OE or mutant effects. On the other hand, viral expression methods are limited in their ability to provide mechanistic insight into the relatively slow etiology of α -synucleinopathies since they produce rapid recapitulation of end-stage nigral cell loss. In light of the field's knowledge about the nature of pathological α -syn and its propagation, a different approach to modeling α -synucleinopathy was recently developed by Volpicelli-Daley et al. utilizing pre-formed fibrils (PFFs) of recombinant α -syn protein (Volpicelli-Daley et al., 2011). Upon powerful pulse sonication, PFFs break up into smaller, oligomeric seeds that induce development of LB-like aggregates both *in vitro* and *in vivo* (Volpicelli-Daley et al., 2011; Luk et al., 2012b). Indeed, the α -syn aggregates that are induced by PFF treatments closely resemble the LBs and LNs found in post-mortem human brains; they are insoluble, proteinase K resistant, phosphorylated at Ser129, ubiquitinated, thioflavin positive, and filamentous in ultrastructure (Volpicelli-Daley et al., 2011; Paumier et al., 2015).

In primary neuronal culture, PFFs are likely taken up by terminals via endocytosis (Volpicelli-Daley et al., 2011), and propagated from neuron-to-neuron by anterograde transport (Freundt et al., 2012). Within four days, PFFs induce formation of punctate α -syn phosphorylated at Ser129 (p-syn) in axons and defects in neuronal synchronization. By ten days, p-syn aggregates become longer and are present in ~25% of cell bodies, with defects in culture excitability and connectivity observed. An increase in autophagy markers is also observed, indicative of the burden

PFFs incur on protein degradation. Fourteen days post-treatment, neurons display reduced presynaptic markers and ~25% neuron death (Volpicelli-Daley et al., 2014).

Several groups have also injected sonicated PFFs into rodent striatum or nigra to examine the utility of the model *in vivo*. Luk et al. (2012) first demonstrated that a unilateral injection of sonicated PFFs into young mice overexpressing p.A53T α -syn under the murine prion promoter (M83 line) is sufficient to accelerate onset of motor symptoms, α -syn pathology in multiple brain regions, and death typically observed at much later time points (Luk et al., 2012b). Soon after, the same group published that unilateral PFF injection in WT mice initiates formation of ipsilateral α -syn pathology in multiple brain regions as soon as 1m post-injection, ipsilateral nigral TH loss at 3m post-injection, and a motor deficit at 3m post-injection (Luk et al., 2012a). Others have since demonstrated that unilateral intrastriatal PFF injection in rats induces ipsilateral α -syn pathology in the striatum and innervating regions at 1m post-injection, bilateral TH loss and striatal innervation at 2m post-injection, bilateral nigral cell loss at 6m post-injection, ipsilateral reductions in striatal DA at 6m post-injection, and ultrasonic vocalization disruption at 6m post-injection (Paumier et al., 2015). Of note, monomer injection also induced disruptions in ultrasonic vocalizations, albeit less severe, suggesting this may be an α -syn protein- and not PFF-induced effect (Paumier et al., 2015). Together, this data suggests that PFF injection can induce a progressive form of α -synucleinopathy in both mice and rats reflected by biochemical, histopathological, and behavioural alterations.

Others have questioned these results and the utility of this acute model. At 4m following unilateral PFF injection into the hippocampus or cortex of mice, Sacino et al. (2014) observed α -syn aggregates surrounding the injection site, but only sparse pathology in interconnected brain regions (Sacino et al., 2014). In addition, they observed that α -syn pathology actually began to

subside at 4m post-cortical injection (Sacino et al., 2014). This finding may be attributable to a smaller PFF injection (2 μ g relative to the previously published 5 μ g in mice) or the use of bath sonication to prepare the PFFs, which may not have sufficiently broken up fibrils into oligomeric seeds. Our own group has electron microscopy data to support this notion (unpublished data), and others have documented that different α -syn strains (i.e. oligomers, fibrils, and ribbons) induce differential behavioural and histopathological consequences when injected into rats (Peelaerts et al., 2015). Dr. Benoit Giasson's group has also repeatedly challenged the use of p-syn as a pathology read-out, as the most commonly used antibody for α -syn phosphorylated at Ser129 (81A) non-specifically binds neurofilament (Sacino et al., 2013, 2014). However, using a suitable co-stain to validate pathology is an acceptable solution to this issue while the field develops a more appropriate pathology read-out. Despite these limitations, the PFF model may have great potential to study progressive and relatively subtle α -synucleinopathy disease processes.

1.5 Rationale for present experiments

The burden of PD to individuals, families, and the greater healthcare system is profound and will escalate with the aging of the Baby Boomer generation. Therefore, the need to develop preventative or therapeutic interventions is of tremendous importance. Attempts to develop treatments for symptomatic patients suffering from neurodegenerative disease have been historically ineffectual, likely due to the progression of pathogenic processes to a point beyond which they can be reversed. A mechanistic understanding of disease etiology appears necessary to identify therapeutic targets before reaching this stage.

Currently, research investigating the relationship between α -syn and LRRK2 is somewhat limited; however, interest appears to be growing within the field. It has been observed that

induction of α -syn pathogenic processes is reduced with LRRK2 KO or kinase inhibition (Lin et al., 2009; Daher et al., 2014, 2015), although these results are based on either extremely aggressive α -syn viral expression or mutant OE of α -syn. Viral expression does not effectively model the slow, progressive disease process as it occurs in patients, and is thus less likely to provide mechanistic insight into disease etiology or a framework for therapeutic trials. Further, mutant OE confounds interpretation of observed consequences, which cannot be definitively attributed to OE or the mutation even with a WT OE control. The PFF model of α -synucleinopathy is a much more suitable model to examine progressive, subtle development of α -syn pathology as it likely occurs in humans, and importantly, provides opportunity for testing efficacy of therapeutic agents at various disease stages. Expression of the p.G2019S mutation has been reported to augment vulnerability to α -synucleinopathy induced by PFFs (Volpicelli-Daley et al., 2016a). With that said, these and other data examining p.G2019S in the context of α -synucleinopathy are limited by caveats of BAC OE of the p.G2019s LRRK2 protein including random gene insertion, parallel exogenous and endogenous expression, and the confounded interpretation of mutant OE-induced consequences. Alternatively, the LRRK2 p.G2019S KI mouse line is a physiologically relevant model in which to study specific consequences of the p.G2019S LRRK2 mutation upon induction of α -syn pathological processes.

This research aims to fill gaps in the current literature by determining a) whether LRRK2 is involved in response to α -syn pathology induced by the relatively subtle PFF model, and b) if endogenous expression of p.G2019S LRRK2 alters this response. This knowledge will enhance the field's understanding of the function of the LRRK2 protein, the consequences of the p.G2019S mutation, and the functional relationship between LRRK2 and pathogenic α -syn. In addition, this research may provide a framework within which to test preventative or therapeutic agents for PD.

2. Methods

2.1 Subjects

Mice were bred and housed at the University of British Columbia Centre for Disease Modeling in compliance with institutional and Canadian Federal Animal Care Committee guidelines. LRRK2 knock-out mice were generated by flanking LRRK2 exon 41 with LoxP sites for deletion with Cre recombinase and maintained on a C57BL6/J background. LRRK2 p.G2019S knock-in mice were created using a loxed PGK-neomycin cassette inserted between LRRK2 exons 41 and 42 and maintained on a C57BL6/J background. All mice were housed in a temperature-controlled unit (21±1°C) on a 12-hour regular light/dark schedule (7am-7pm light). Weaning occurred at ~23 days postnatal, and mice were housed with up to 5 same-sex littermates in clear cages with basic enrichment (bedding material, nesting material, and a nesting dome). Animals were provided *ad libitum* access to food and water. Primary neurons were acquired from embryos of both sexes for cultures. Only male mice were used for *in vivo* experiments.

2.2 Primary neuronal culture and nucleofection

At E16.5-17.5, pregnant mice heterozygous for the LRRK2 p.G2019S mutation were killed by CO₂ exposure. Brains were dissected from pups and placed into 1ml Hibernate-E medium supplemented with B-27 on ice. Tail samples from embryos were genotyped using PCR and confirmed as being wild-type (WT), heterozygous for the LRRK2 p.G2019S mutation (Het), or homozygous for the LRRK2 p.G2019S mutation (Homo) prior to grouping of brains by genotype. Cortices were microdissected with Hank's Balanced Salt Solution supplemented with 0.03% D-glucose, 0.01% HEPES buffer, and 0.01% penicillin/streptomycin (HBSS+), and subject to trypsin digestion using 0.05% Trypsin-0.25% EDTA for 10min at 37°C. Following addition of trypsin

inhibitor, cells were centrifuged and resuspended with neurobasal medium supplemented with 0.02% B-27 and 0.0025% L-glutamine (NBM+) and DNase I. Tissue was thoroughly triturated and re-centrifuged before neurons were counted. Neurons were seeded at a density of 250 000 cells/well in 1mL NBM+ on microscope cover slips in a 24-well plate or 1 000 000 cells/well in 2mL NBM+ in a 6-well plate. Plates were coated with poly-D-lysine.

To visualize individual neurons, some cultures were induced to express a GFP fill by nucleofection at DIV0; following cell counting, cortical neurons were pelleted by centrifugation followed by resuspension in electroporation buffer (Mirus) and 1 μ g/million cells pAAV-GFP-CAG plasmid (Adgene, 37825). The suspension was placed into a cuvette and electroporated using an Amaxa Nucleofector2b (Lonza). Nucleofected cells were added to an equal number of non-nucleofected cortical neurons in NBM+ and plated in a 24-well plate at a density of 250 000 cells/well. All cultures were maintained at 37°C in a humidified incubator with 5% CO₂. After DIV4, an additional 10% of media was added to each well every 4-5 days.

2.3 Electron microscopy

Electron microscopy was utilized for qualification of PFFs pre- and post-sonication. Both unsonicated and sonicated PFF dilutions were adsorbed onto carbon-coated 200-mesh grids and subject to negative staining with 1% uranyl acetate. Images were generated using a transmission electron microscope (TEM; FEI, Technai G2 Spirit model).

2.4 Culture pre-formed fibril treatments

α -Syn PFFs were generously donated by Dr. Laura Volpicelli-Daley, University of Alabama at Birmingham, who qualified each batch by performing sedimentation, electron

microscopy, thioflavin T, and endotoxin assays. Immediately before treatment at DIV7, PFFs diluted in phosphate-buffered saline (PBS) were subject to sonication with a probe tip sonic dismembrator (Fischer Scientific, model 120) for 30s (1s on, 1s off) at 50% maximum power. Treatment was performed by depositing 0.5mL of media from each well into a 15mL Falcon tube corresponding to its condition (WT PBS, WT PFF, mutant PBS, or mutant PFF), adding PBS or PFFs to the removed media (final PFF concentration of 2 μ g/mL), and re-adding the media.

2.5 Lactate dehydrogenase assay

Cell integrity was assessed using a lactate dehydrogenase (LDH)-based colorimetric toxicity assay (Sigma) at DIV9 (2d post-treatment), DIV12 (5d post-treatment), and DIV17 (10d post-treatment). Media from wells of each condition was deposited into separate Eppendorf tubes. Positive (media from a well exposed to 8% TritonX-100) and negative (serum-free media) controls were included. Tubes underwent brief centrifugation to sediment any cell debris. Supernatant was removed and mixed thoroughly with one part NAD⁺ substrate, one part reduction co-factor, and one part NADH-interacting probe (λ_{max} =450nm). Solution from each condition was added to a 96-well plate in triplicate and left to incubate for 30min. A microplate reader detected the optical density of each well. Condition triplicates were averaged and the serum free media value was subtracted.

2.6 Immunocytochemistry

At DIV17, neurons were fixed in 4% paraformaldehyde (PFA) and 4% sucrose for 15min followed by three 10min PBS washes. Neurons were blocked for 1h using 5% normal goat serum (NGS; Gibco, 16210-072) in PBS. Primary antibodies were diluted in an antibody solution of 2%

NGS in PBST (0.2% Tween-20). After overnight incubation at 4°C, neurons were washed with blocker for an additional hour. Secondary antibodies (Alexa-488 and Alexa-568 conjugated α -rabbit and α -mouse, Molecular Probes) were diluted in antibody solution (1:1000) and incubated in the dark for 30min followed by three 10min PBS washes. Coverslips were mounted with fluoromount (Southern Biotech).

Primary antibodies included: rabbit anti-GFP (1:1000; Abcam, ab6556), chicken anti-GFP (1:1000; Abcam, ab13970), rabbit anti-GFAP (1:1000; Abcam, ab7260), goat anti-Iba1 (1:1000; Novus Biologicals, NB100-1028), rabbit anti-p62 (1:500; Abcam, ab91526), rabbit anti-LAMP1 (1:250; Abcam, ab24170), and mouse anti-p-syn (1:1000; Abcam, ab184674).

2.7 Fluorescence imaging and analysis

Images taken for DAPI and field p-syn quantification were obtained with an EVOS FL Auto Imaging System and acquired at 40x magnification. Images taken for field p62 and LAMP1 quantification, cell body stain quantification, and co-localization were obtained with an Olympus Fluoview 1000 confocal microscope and acquired as 1 μ m z-stacks at 60x magnification. For DAPI quantification, images were binarized using ImageJ and a CellProfiler pipeline designed to recognize circular objects was used to count nuclei. Manual scoring was used to count condensed nuclei. For field stain quantification, images were thresholded using Photoshop (Adobe), the mean gray value for each image was quantified using ImageJ, and values were normalized to average density of healthy nuclei within that condition. Affected cell bodies in each condition were counted manually and normalized to the average density of healthy nuclei within that condition. Affected cell bodies were masked out of all images for neuritic p-syn quantification, and subsequently performed in the same way as field quantification. For cell body p-syn, p62, and LAMP1

quantification, images were thresholded using Photoshop, regions of interest (ROIs) were drawn by hand using ImageJ, and mean gray value was quantified. For protein co-localization analysis, images were thresholded using Photoshop and Pearson's R coefficient was calculated using Fiji. Acquisition and analysis parameters were constrained within each culture.

2.8 Behavioural testing

2.8.1 Apparatus

For the cylinder test, 11 glass beakers were placed in front of a Webcam for trial recording and post-hoc scoring.

For the open field and novel object location (NOL) tests, a 48cm x 48cm (L x W) Plexiglas compartment (TSE Systems) was decorated with simple cues on each wall and placed under a Webcam for trial recording and post-hoc tracking. The objects utilized for NOL included a green mug and blue bottle, each of similar size (15x8.5cm and 17.5x6cm) and texture.

The puzzle box test was performed in the dark so that an aversive light stimulus would motivate the mice to enter a dark chamber. A 57cm x 27cm (L x W) white Plexiglas compartment (Stoelting) with a small entrance to a dark chamber was placed under a bright light as well as a Webcam for trial recording and post-hoc tracking. One simple cue was placed above the chamber entrance. Nesting material was placed in the dark chamber to provide additional motivation for the mouse to enter in subsequent trials. A number of additive changes to the apparatus were made to increase the difficulty of chamber entry following the first trial: 1) the dark chamber entry hole was made smaller by placing a Plexiglas panel insert in front of the entry, 2) a pile of bedding material was placed at either end of the compartment to obstruct entry, and 3) the compartment was rotated 180° and the cue was moved to the opposite wall.

2.8.2 Testing paradigms

Mice were handled for 3 days prior to behavioural testing so that they would become accustomed to the experimenter's touch. For the cylinder test, a mouse was placed into a glass beaker and allowed to move about freely for 5min before being returned to its home cage. Cylinders were thoroughly washed with water between trials.

For the open field test, a mouse was placed into the open field/NOL Plexiglas compartment and allowed to explore for 15min before being returned to its home cage for a period of 5-20min. Two objects were placed into the compartment, and the mouse was allowed to explore freely for 5min for trial 1 (T1) of NOL. Following a 24h delay, one of the objects was moved to a new location and the mouse was allowed to explore for 5min for trial 2 (T2) of NOL. Compartments and objects were thoroughly washed with 70% ethanol and water between trials.

For the puzzle box test, the mice completed a total of nine trials over three days (three trials/day). For each trial, a mouse was placed into the puzzle box Plexiglas compartment facing west and allowed to search for the dark chamber. The mouse was left in the dark chamber for 1.5min after entry to provide motivation for entry in subsequent trials, and then returned to its home cage for a period of 1h between trials occurring on the same day. No changes were made to the behavioural apparatus for T1. For T2 and T3, the panel insert was utilized to make the dark chamber entry smaller. After a 24h delay period, the mouse completed T4 using the same conditions as T2/T3. For T5 and T6, bedding material was introduced such that the mouse had to dig its way through to reach the dark chamber. After a 24h delay period, the mouse completed T7 using the same conditions as T5/T6. For T8 and T9, the apparatus was rotated 180° and the cue was moved to the opposite side of the compartment. The compartment and insert were thoroughly washed with 70% ethanol and water between trials.

2.8.3 Scoring and analysis

For the cylinder test, the following measures were acquired by manual scoring: rearing number, number of forepaw uses, number of grooming events, and time spent grooming. For the open field and NOL tests, videos were scored using ANY-maze tracking software (Stoelting). Acquired data included distance travelled, time mobile, entries to centre, time spent in centre, distance travelled in centre, and time mobile in centre for open field. For the NOL test, time spent investigating the familiar object and novel object was also acquired, where investigation was defined as nose entry to the region immediately surrounding the object. For the puzzle box test, time taken to enter the dark chamber was acquired manually.

2.9 Stereotaxic surgery

Mice were weighed prior to surgery for a post-surgical monitoring reference. Anesthetization was achieved by administration of 5% vaporized isoflurane and medical grade oxygen in an induction chamber, and confirmed by performing the rear foot reflex test. Each mouse was secured in stereotaxic ear bars (David Kopf Instruments) over a heating pad, and received 2-2.5% isoflurane routed to the incisor adaptor to maintain a surgical plane of anesthesia. Throughout the surgery, each mouse's level of anesthesia was monitored by observing breathing rate and temperature, and isoflurane administration was adjusted accordingly. Lubricating ointment (Refresh Lacri-Lube) was applied to the mouse's eyes prior to shaving and sterilization of the scalp with 70% ethanol and iodine. Local analgesic (Metacam) was administered between the ears at a concentration of 0.5µl/g. A small incision was made through the skin along the midline to expose the skull. A micromotor drill (Stoelting) with a 0.5mm drill bit was positioned above the bregma using optical guidance, and steered by Stereodrive software (Neurostar) to the x (+0.5mm AP) and

y (+2.1mm ML) coordinates of the right dorsolateral striatum (Paxinos and Franklin, 2004). Under optical guidance, a hole was drilled to the inner surface of the skull, with care taken to not damage the dura mater. A needle pre-constructed from silica capillary tubing (outer diameter 150 μ m, Polymicro Technologies) stabilized by a guide cannula (Bilany) was slowly lowered into the brain to reach the y coordinate (-2.8mm DV) of the dorsolateral striatum. The injection material (2 μ l of 2.5 μ g/ μ l PFFs or 2 μ l PBS) was infused at a rate of 1 μ g/min through fine bore tubing (Smiths Medical) from a gas-tight 500 μ l syringe (Hamilton Company) using a syringe pump (CMA, Harvard Apparatus). A subcutaneous injection of 0.5mL saline (0.9%) was administered for fluid loss prevention. After the injection was complete, the needle was slowly retracted and the injection site was cleaned with PBS. The skin was sutured with Monocryl 4-0 (Ethicon) and secured with tissue adhesive (Vetbond). The mouse was placed in a warm recovery cage until awake and motile, then returned to its home cage. The weight, appearance, and behaviour of each mouse was monitored for at least 5 days following surgery. Analgesic was administered if any animal appeared to display signs of pain.

2.10 Statistics

Following software analysis or manual scoring, data was imported into GraphPad Prism. Two-tailed t-tests were run for comparison of two groups, and ANOVA tests followed by Bonferroni's post-hoc test were run for comparisons of over two groups ($\alpha=0.05$). Power analyses were conducted using GraphPad Statmate ($\alpha=0.05$).

3. Results

3.1 Induced α -synucleinopathy in primary neurons by pre-formed fibril treatment

PFFs were examined by TEM pre- and post-sonication to confirm presumed ultrastructure (Figure 1). Primary cortical neurons from WT, LRRK2 KO (herein referred to as KO), or Homo LRRK2 p.G2019S KI (herein referred to as KI) embryos were treated with PBS, 1 μ g/ml α -syn monomer, or 1 μ g/ml sonicated PFFs at DIV7 and fixed at DIV17 after 10d treatment. The LDH assay was performed using media from each condition to examine cell membrane integrity. Fixed neurons were subject to immunocytochemistry to examine levels of p-syn, co-localization of p-syn with cellular markers, and neuronal density. Any differences in induced α -synucleinopathy between genotypes were shown to be purely neuronal as demonstrated by the absence of Iba1 and GFAP staining in cultures (data not shown).

3.1.1 Monomeric α -synuclein does not induce α -synucleinopathy

Primary cortical neurons from WT embryos were treated with a PBS vehicle control or 1 μ g/ml α -syn monomer at DIV7, fixed at DIV17, and subject to immunocytochemistry. p-Syn staining (evident in PFF-treated cultures, see 3.1.2) was found to be negligible in both PBS-treated neurons and α -syn monomer-treated neurons in two separate cultures (Figure 2).

3.1.2 Leucine-rich repeat kinase 2 knock-out neurons are protected from pre-formed fibril-induced α -synucleinopathy

Primary cortical neurons from WT and KO embryos were treated with PBS or 1 μ g/ml sonicated PFFs at DIV7, fixed at DIV17, and subject to immunocytochemistry. In agreement

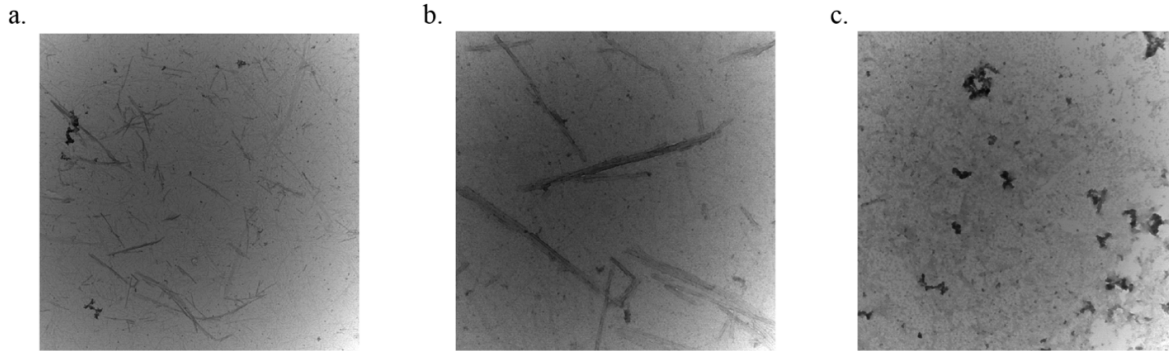


Figure 1. Transmission electron microscopy of α -synuclein pre-formed fibrils pre- and post-sonication.

Prior to mechanical disruption with a probe tip sonicator, PFFs were observed to have a fibrillar ultrastructure (**a-b**). After sonication, PFFs appeared non-fibrillar, although oligomeric forms clearly remain (**c**). Images **a** and **c** were taken at 16 500x; **b** was taken at 24 500x. PFF= α -synuclein pre-formed fibril.

were observed in PFF treatment conditions compared to PBS treatment conditions ($p < 0.0001$) in WT neurons. p-Syn staining was found to be present mostly in axons, but also appeared pronounced in a small percentage (~5%) of cell bodies (Figure 3). Further demonstrating this, p-syn was observed to co-localize with tau-positive axonal compartments as previously reported (Volpicelli-Daley et al., 2016a), but not MAP2-positive dendritic compartments as expected following 10d of treatment (Volpicelli-Daley et al., 2014) (data not shown).

Interestingly, there was significantly less p-syn staining in PFF-treated KO neurons relative to WT neurons in five separate cultures ($p = 0.01$) (Figure 4a). To examine whether differences in PFF-induced cell death contributed to genotypic differences in p-syn staining, general culture health was assessed by performing the LDH assay on culture media at DIV17 and manual condensed nuclei counts. A non-significant increase in cell death was observed in PFF-treated relative to PBS-treated conditions by the LDH assay, with a potential reduction in basal KO cell death (Figure 4b). LDH assay results were also similar between genotypes at DIV9 and DIV12 (data not shown). In agreement with the LDH assay, the density of condensed/pyknotic nuclei, which indicate the beginning of cell death processes (Kroemer et al., 2009), showed no significant differences between genotypes or treatments (Figure 4c). Together, these data suggest that

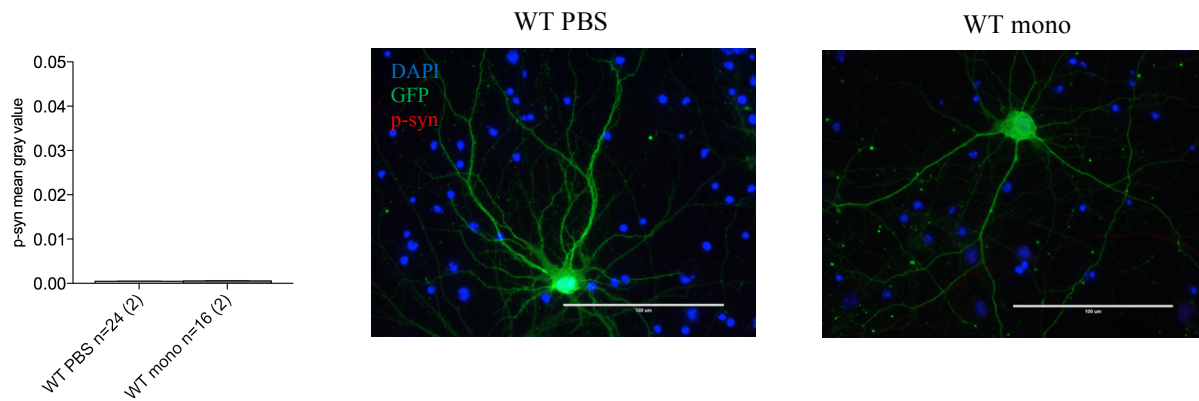


Figure 2. Treatment with α -synuclein monomer does not induce α -synucleinopathy.

Primary cortical cultures containing a sub-population of GFP-expressing neurons for visualization of cell morphology were treated with PBS (vehicle control) or α -syn monomer (synuclein control) at DIV7, neurons showed negligible p-syn staining at DIV17. Representative images shown are stained for DAPI (nuclei), GFP (cell fill) and p-syn (pathological synuclein). Experimental ‘n’ indicates number of image fields with number of independent cultures in brackets. Error bars represent standard errors of the mean. GFP=green fluorescent protein, mono= α -synuclein monomer, PBS=phosphate buffered saline, p-syn= α -synuclein phosphorylated at serine 129, WT=wild-type.

reduced p-syn staining in KO cultures cannot be accounted for by increased neuronal death.

To further probe the mechanism of this protection, cell bodies in which p-syn-positive aggregates were present (affected cell bodies, ACBs) were compared between genotypes. The number of ACBs was less in PFF-treated KO neurons relative to WT neurons, but this strong trend failed to reach statistical significance ($p=0.054$) (Figure 4d). Individual ACBs had similar levels of p-syn staining between genotypes (Figure 4e). Excluding ACBs from images prior to p-syn quantification revealed KO neurons also had a strong trend towards reduced p-syn staining in neurites (Figure 4f), but again, this was just below the level of statistical significance ($p=0.092$). Together, these data suggest that p-syn reduction in KO neurons is a compound effect of less p-syn in neurites and fewer cells with somatic inclusions, although similar staining is present within ACBs when they do contain aggregates. It may be that KO cultures exhibit protection against PFFs by a) less efficient fibril uptake, b) more effective neuritic degradation of pathogenic α -syn, or c) less efficient neuron-to- neuron spread of pathogenic α -syn.

The autosome-lysosome system is one of the two primary degradation mechanisms of the cell, and has been proposed to be the predominant pathway by which α -syn degradation occurs.

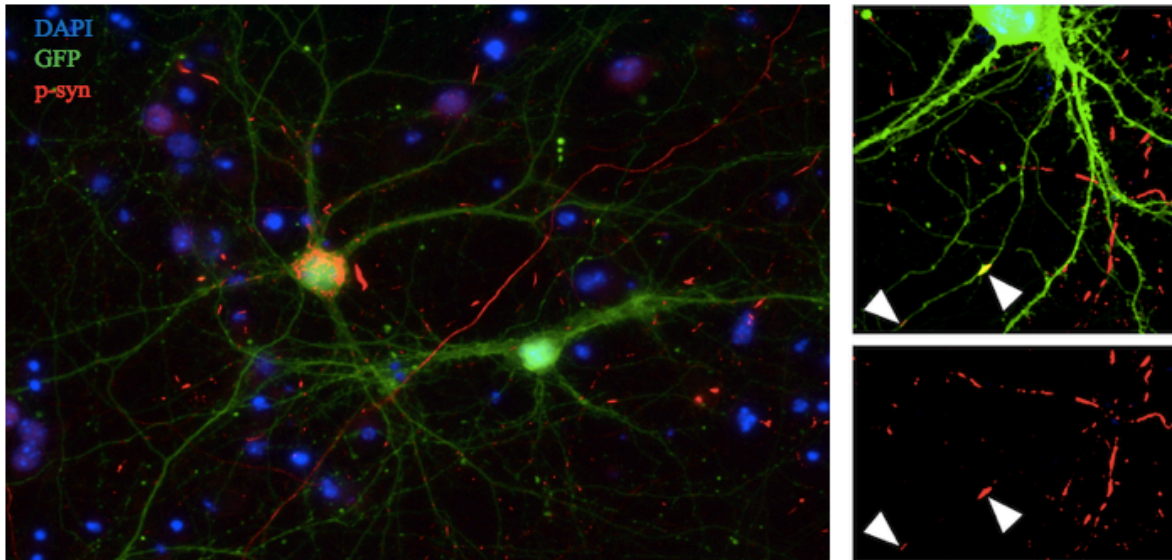


Figure 3. Basic characterization of pre-formed fibril treatment in primary neurons.

Primary cortical cultures containing a sub-set of cells expressing GFP for visualisation of cell morphology were administered PBS or PFFs at DIV7. Cells were fixed for analysis of PFF-induced α -synucleinopathy by immunofluorescence at DIV17. A small percentage of neurons had pronounced p-syn accumulation in the cell body, (left). However, the vast majority of staining was within axonal processes of both GFP-filled and unfilled cells, suggestive of retrograde pathology beginning in axon terminals and progressing towards the cell body (right, arrows). DIV=days *in vitro*, GFP=green fluorescent protein, PBS=phosphate buffered saline, PFF=pre-formed fibril, p-syn= α -synuclein phosphorylated at serine 129, WT=wild-type.

Its dysfunction has been implicated in PD and specifically in accumulation of α -syn (Desplats et al., 2009). To examine potential genotypic differences in autophagy and lysosomal markers, staining of p62 (which is proposed to recognize ubiquitinated proteins and inclusions destined for autophagy; Bjorkoy et al., 2005; Pankiv et al., 2007) and LAMP1 in ACB-containing fields was conducted in a respective total of three and two KO cultures (Figure 5, 6). p62 appeared slightly increased in WT and KO PFF-treated neurons relative to PBS controls (Figure 5a), but the effect was not significant. Further, p-syn appeared to co-localize with p62 to a comparable extent in PFF-treated WT (Pearson's $R=0.24$) and KO (Pearson's $R=0.32$) neurons (Figure 5b). KO PBS-treated neurons showed a strong trend towards increased LAMP1 signal relative to WT PBS-treated neurons, suggesting there may be intrinsically higher levels of LAMP1 clustering in KO cultures ($p=0.08$) (Figure 6). Consistent with this observation, WT PFF-treated neurons showed a

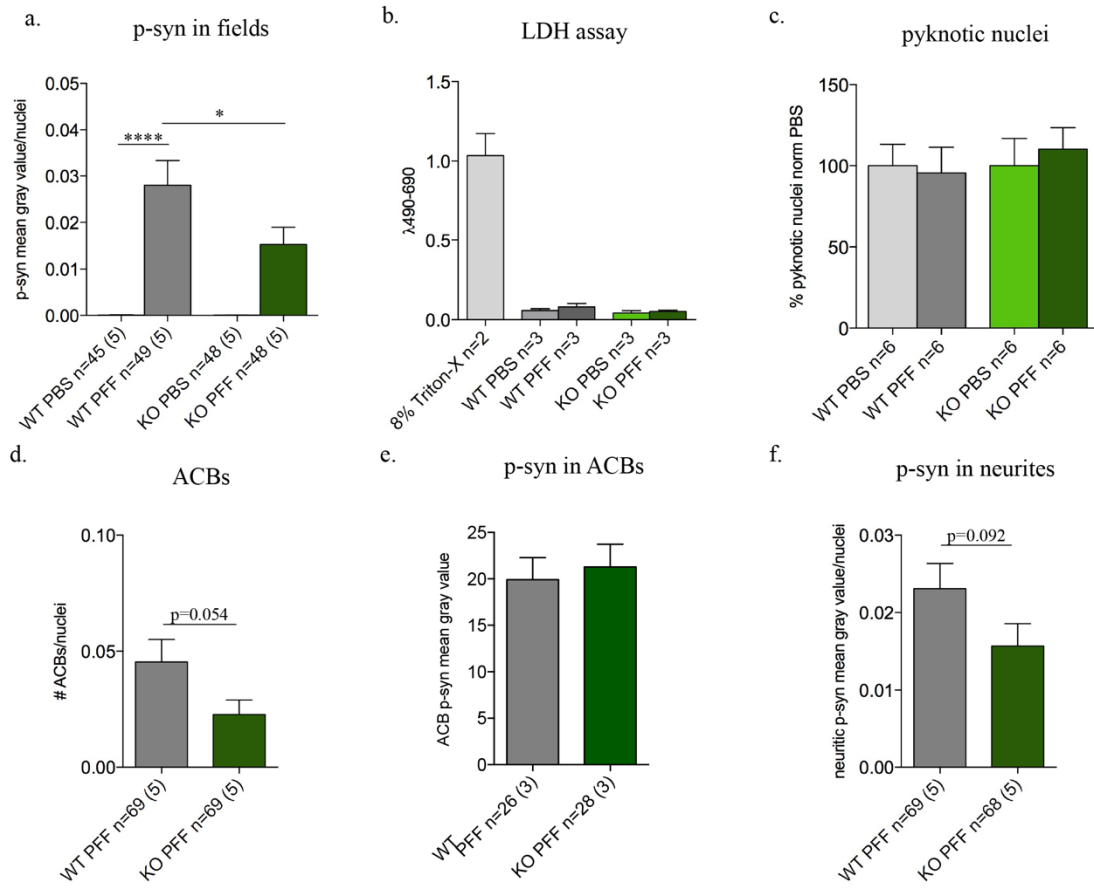
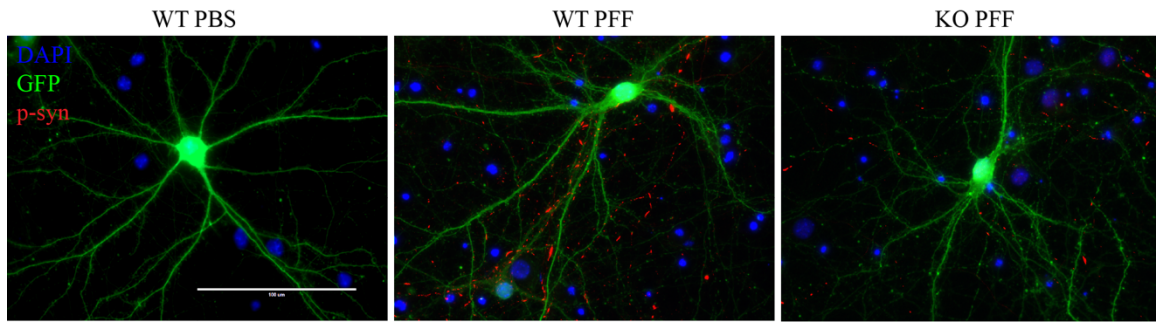


Figure 4. Pre-formed fibril treatment of leucine-rich repeat kinase 2 knock-out primary neurons.

Following treatment with PBS or PFFs at DIV7, PFF-treated neurons showed significantly higher p-syn staining than PBS-treated neurons by DIV17 (a). Further, PFF-treated KO neurons showed significantly lower p-syn staining than PFF-treated WT neurons (a). No significant differences in toxicity were observed between conditions as measured by the LDH assay (b) or the percentage of pyknotic nuclei (c). The number of ACBs was lower in PFF-treated KO neurons relative to WT, but not significantly (d). While the area of p-syn staining in ACBs was similar in WT and KO ACBs (e), KO neurites trended towards less p-syn in neurites (p=0.092). p-Syn field and neuritic values are reported as mean gray value normalized to nuclear density of each condition. Pyknotic nuclei values are reported as the number of pyknotic nuclei as a percent of the total number of nuclei in each condition normalized to PBS control. ACBs are reported as the number of cell bodies with clear p-syn staining normalized to nuclear density of each condition. Experimental ‘n’ indicates number of image fields with number of independent cultures in brackets. Error bars represent standard errors of the mean. ACB=affected cell body, GFP=green fluorescent protein, KO=leucine-rich repeat kinase 2 knock-out, LDH=lactate dehydrogenase, p-syn= α -synuclein phosphorylated at serine 129, PBS=phosphate buffered saline, PFF=pre-formed fibril, WT=wild-type. *p<0.05, ****p<0.0001 by one-way ANOVA and Bonferroni’s post-hoc test in a; *p<0.05 by two-tailed t-test in d and f.

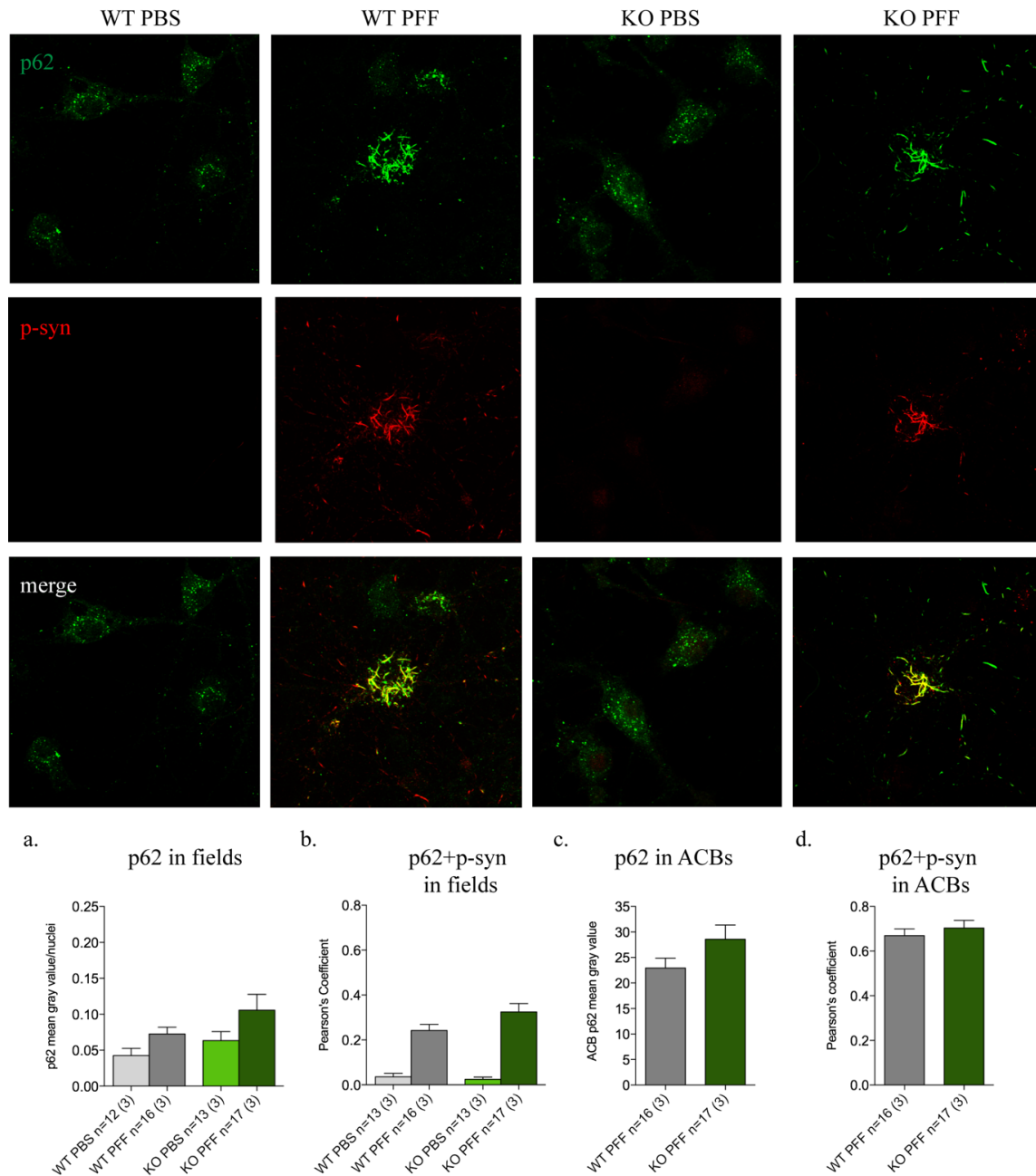


Figure 5. The autophagy marker p62 in pre-formed fibril-treated leucine-rich repeat kinase 2 knock-out primary neurons.

Following treatment with PBS or PFFs at DIV7, PFF-treated neurons showed a trend towards higher p62 staining relative to PBS-treated neurons (a). p62 levels in fields and in ACBs were not significantly different between WT and KO neurons (a, c). p-Syn co-localized with p62 modestly in WT (Pearson's R=0.24) and KO (Pearson's R=0.32) fields and highly in WT (Pearson's R=0.67) and KO (Pearson's R=0.70) ACBs (b, d). p62 field values are reported as mean gray value normalized to nuclear density of each condition. Experimental 'n' indicates number of image fields with number of independent cultures in brackets. Error bars represent standard errors of the mean. ACB=affected cell body, KO= leucine-rich repeat kinase 2 knock-out, p62=sequestosome 1, p-syn= α -synuclein phosphorylated at serine 129, PBS=phosphate buffered saline, PFF=pre-formed fibril, WT=wild-type.

Significant increase in LAMP1 relative to PBS-treated neurons ($p=0.02$), whereas KO PFF-treated neurons did not (Figure 5a). p-Syn co-localized with LAMP1 to some extent in PFF-treated WT (Pearson's $R=0.09$) and KO (Pearson's $R=0.10$) neurons with no genotypic difference (Figure 6b).

Both p62 and LAMP1 appeared to primarily localize to ACBs in PFF-treated neurons. Therefore, p62 and LAMP1 levels as well as each protein's co-localization with p-syn were examined in ACBs specifically. p62 and LAMP1 levels as well as each protein's co-localization with p-syn were increased in KO ACBs relative to WT, albeit non-significantly (Figure 5c, 6c). p62 was highly co-localized with p-syn in ACBs of both WT (Pearson's $R=0.67$) and KO (Pearson's $R=0.70$) neurons (Figure 5d). LAMP1 appeared to co-localize with p-syn somewhat less in WT (Pearson's $R=0.31$) and KO (Pearson's $R=0.30$) fields, also with no significant difference between genotypes (Figure 6d).

3.1.3 p.G2019S leucine-rich repeat kinase 2 knock-in neurons are more susceptible to pre-formed fibril treatment-induced α -synucleinopathy

Primary cortical neurons from WT and KI neurons were treated with PBS or $1\mu\text{g/ml}$ sonicated PFFs at DIV7, fixed at DIV17, and subject to immunocytochemistry. As previously reported, p-syn staining was significantly higher in WT PFF relative to PBS conditions in five separate cultures ($p<0.0001$) (Figure 7a). In addition, the level of p-syn staining was significantly higher in KI neurons relative to WT neurons treated with PFFs in four separate cultures ($p=0.005$) with comparable death observed across conditions of the same culture (Figure 7a, b).

To further probe the mechanism of KI susceptibility, ACBs were compared between genotypes. The number of ACBs was comparable in PFF-treated WT and KI neurons (Figure 7c), suggesting that WT and KI neurons uptake PFFs and spread pathogenic α -syn from neurites to the

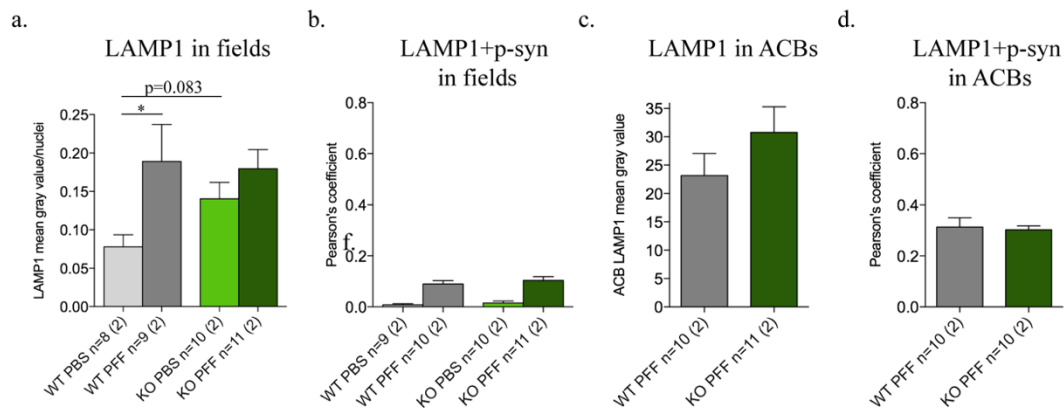
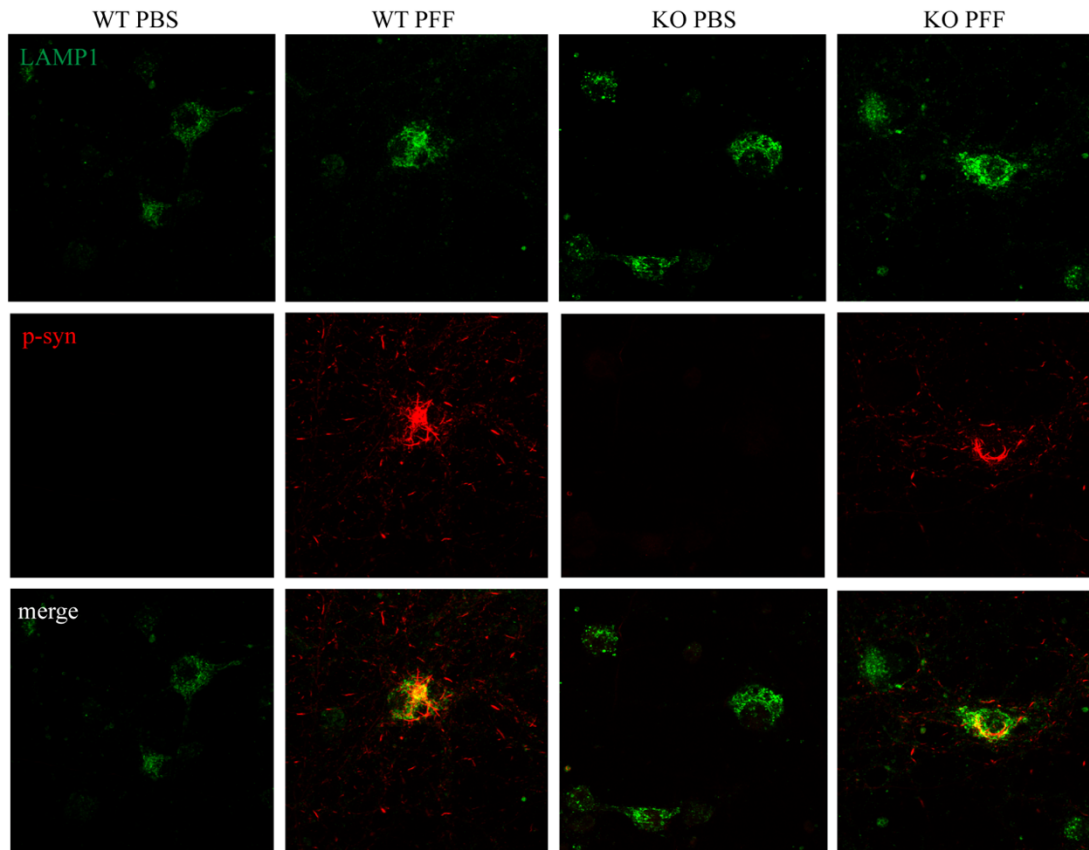


Figure 6. The lysosomal marker LAMP1 in pre-formed fibril-treated leucine-rich repeat kinase 2 knock-out primary neurons.

Following treatment with PBS or PFFs at DIV7, KO PBS-treated neurons showed a strong trend towards higher LAMP1 levels relative to WT PBS-treated neurons (a). WT PFF-treated neurons had significantly higher LAMP1 levels relative to PBS where KO PFF-treated neurons did not (a). LAMP1 levels did not differ significantly between WT and KO PFF-treated neurons in fields or ACBs (a, c). In PFF-treated conditions, p-syn co-localized with LAMP1 to some degree in WT (Pearson's $R=0.09$) and KO (Pearson's $R=0.10$) fields, and to a slightly higher degree in WT (Pearson's $R=0.31$) and KO (Pearson's $R=0.30$) ACBs (b, d). LAMP1 field values are reported as mean gray value normalized to nuclear density of each condition. Experimental 'n' indicates number of image fields with number of independent cultures in brackets. Error bars represent standard errors of the mean. ACB=affected cell body, KO=leucine-rich repeat kinase 2 knock-out, LAMP1=lysosomal membrane-associated protein 1, p-syn= α -synuclein phosphorylated at serine 129, PBS=phosphate buffered saline, PFF=pre-formed fibril, WT=wild-type. * $p<0.05$ by one-way ANOVA and Bonferroni's post-hoc test.

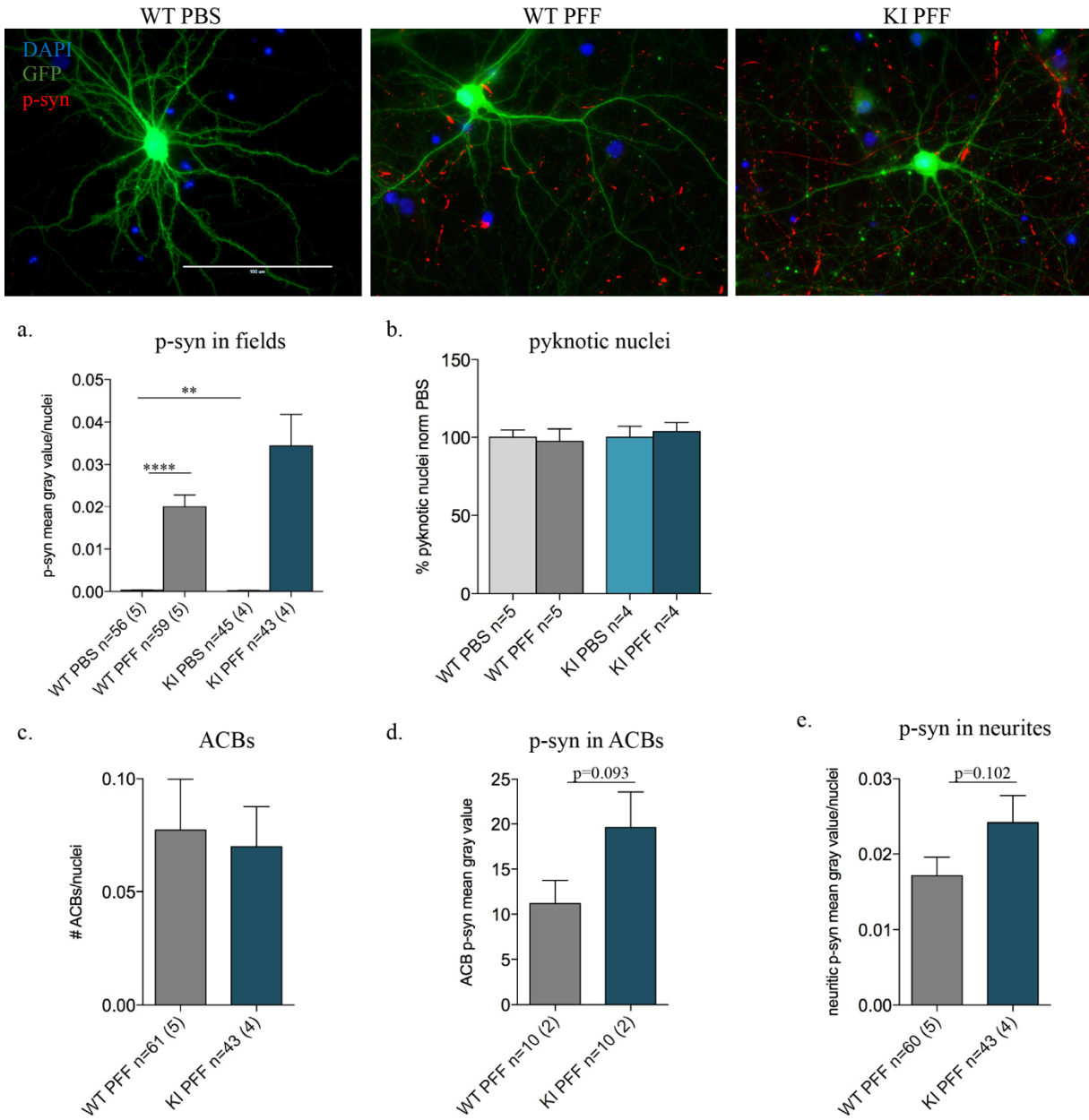


Figure 7. Pre-formed fibril treatment of leucine-rich repeat kinase 2 p.G2019S knock-in primary neurons.

Following treatment with PBS or PFFs at DIV7, PFF-treated neurons showed profoundly higher p-syn staining than PBS-treated neurons by DIV17 (a). In addition, PFF-treated KI neurons showed significantly higher p-syn staining than PFF-treated WT neurons (a). No differences in the percentage of pyknotic nuclei between conditions were observed (b). While the number of ACBs was similar between PFF-treated WT and KI neurons (c), the amount of p-syn staining in KI ACBs (d) and neurites (e) appeared greater, albeit not significantly ($p=0.093$, 0.102). p-Syn field and neuritic values are reported as mean gray value normalized to nuclear density of each condition. Pyknotic nuclei values are reported as the number of pyknotic nuclei as a percent of the total number of nuclei in each condition normalized to PBS control. ACBs are reported as the number of cell bodies with marked p-syn staining normalized to nuclear density of each condition. Experimental ‘n’ indicates number of image fields with number of independent cultures in brackets. Error bars represent standard errors of the mean. ACB=affected cell body, GFP=green fluorescent protein, KI=leucine-rich repeat kinase 2 p.G2019S knock-in, p-syn= α -synuclein phosphorylated at serine 129, PBS=phosphate buffered saline, PFF=pre-formed fibril, WT=wild-type. $**p<0.01$, $****p<0.0001$ by one-way ANOVA and Bonferroni’s post-hoc test; $*p<0.05$ by two-tailed t-test in d and e.

cell body with similar efficiency. However, p-syn staining in ACBs ($p=0.093$) and neurites ($p=0.102$) appeared higher in KI neurons relative to WT, cumulatively contributing towards the significant overall p-syn stain increase in KI neurons (Figure 7d, e). This suggests that KI cultures might be generally more susceptible to induced α -synucleinopathy within each cell by intrinsically less effective handling of pathogenic α -syn.

p62 staining was examined in one full culture and one partial culture to investigate potential differences in this marker of autophagy (Figure 8). Intriguingly, p62 appeared to be intrinsically upregulated in PBS-treated KI neurons relative to PBS-treated WT neurons ($p=0.003$); however, small sample size must be taken into consideration when interpreting these results (Figure 6a). p62 staining was significantly increased in PFF-treated WT neurons relative to PBS-treated WT neurons ($p=0.03$), but not different between PBS- and PFF-treated KI neurons (Figure 6a). There was no significant difference in p62 levels of PFF-treated WT and KI neurons (Figure 6a). This may suggest that KI neurons have inherently altered degradation processes, and are already subject to increased autophagic activation. In addition, p62 co-localized with p-syn to a significantly greater extent in PFF-treated KI neurons (Pearson's $R=0.43$) relative to PFF-treated WT neurons (Pearson's $R=0.19$) ($p=0.001$) (Figure 6c). Though this may be a result of increased levels of p-syn and p62 levels in KI neurons, it may also reflect differential handling of pathogenic α -syn following treatment with PFFs.

As in KO cultures, p62 levels and co-localization with p-syn specifically in ACBs were examined. p62 levels appeared to be similar in both genotypes (Figure 6b). The protein appeared to co-localize well with p-syn in WT (Pearson's $R=0.48$) and KI (Pearson's $R=0.60$) ACBs, though this difference was not significant (Figure 6d).

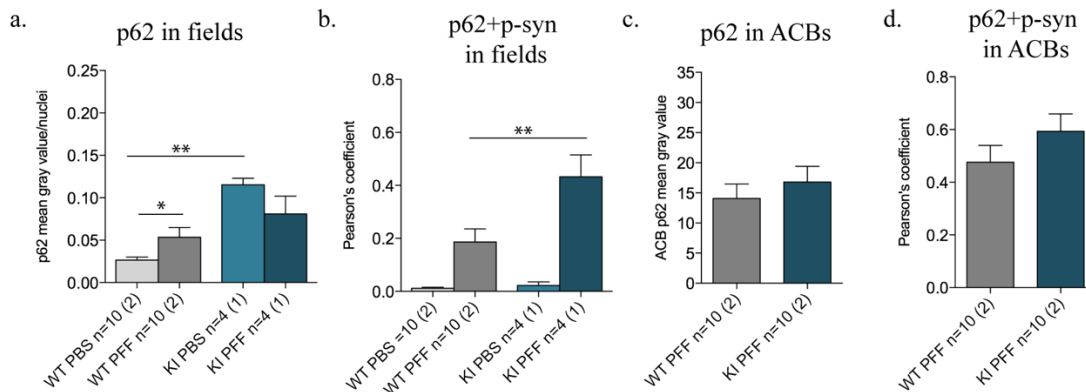
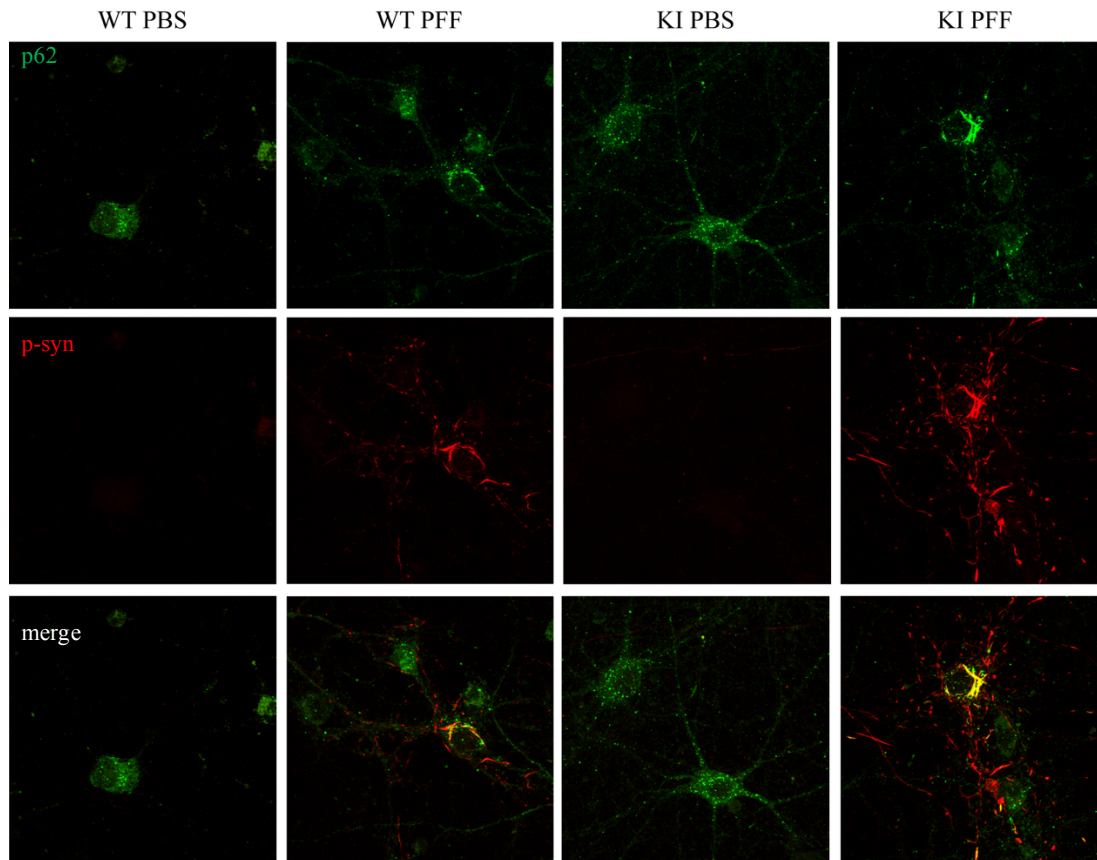


Figure 8. The autophagy marker p62 in pre-formed fibril-treated leucine-rich repeat kinase 2 p.G2019S knock-in primary neurons.

Following treatment with PBS or PFFs at DIV7, KI PBS-treated neurons showed significantly higher p62 staining relative to WT PBS-treated neurons (a). WT PFF-treated neurons showed significantly higher p62 staining relative to PBS-treated neurons, while KI PFF-treated did not (a). p62 levels in ACBs were comparable in WT and KI neurons (b). In fields, p-syn co-localized with p62 to a significantly greater extent in KI (Pearson's $R=0.43$) than in WT (Pearson's $R=0.19$) PFF-treated neurons (c). In ACBs, co-localization of p-syn and p62 co-localization was not significantly different between PFF-treated WT (Pearson's $R=0.48$) and KI (Pearson's $R=0.60$) neurons (d). p62 field values are reported as mean gray value normalized to nuclear density of each condition. Experimental 'n' indicates number of image fields with number of independent cultures in brackets. Error bars represent standard errors of the mean. ACB=affected cell body, KI=leucine-rich repeat kinase 2 p.G2019S knock-in, p62=sequestosome 1, p-syn= α -synuclein phosphorylated at serine 129, PBS=phosphate buffered saline, PFF=pre-formed fibril, WT=wild-type. * $p<0.05$, ** $p<0.01$ by one-way ANOVA and Bonferroni's post-hoc test.

3.2 Induced behavioural deficits in mice by intrastriatal pre-formed fibril injection

To gain a holistic behavioural characterization against which to test the effects of PFF injections, mice underwent behavioural testing designed to quantify motor, anxiety, and cognitive performance over the course of this experiment. The data presented here contribute to a pilot experiment, and power analyses were conducted to calculate by power analyses the sample size required for subsequent *in vivo* PFF experiments. Although this cohort only provides preliminary data, the results appear to be quite promising.

Animals were subject to the cylinder test to examine vertical motor exploration and anxiety-like behaviours, where rearing and forelimb contacts against the cylinder wall indicated motor activity, and grooming behaviours indicated anxiety levels. The open field test also provided motor and anxiety measures; specifically, distance travelled assays general locomotor function, whereas the centre path ratio (i.e. percentage of total distance travelled that was in the centre area) indicates anxiety-like behaviours by providing a measure of relative thigmotaxis. Mice were also tested in the NOL and puzzle box paradigms to examine cognitive abilities. In the NOL test, cognitive ability was assumed to be intact if mice spent more time investigating an object moved to a novel location than with an object that did not move location following a 24h delay period. As rodents are known to prefer novelty, failure to discriminate between objects in a novel vs. familiar location likely indicates a deficit in memory and/or motivation, both required to demonstrate 'learning' in this task. The puzzle box demonstrated ability to a) learn increasingly difficult dark chamber entry strategies in T2 (introduction of a small entry), T5 (introduction of a bedding obstruction), and T8 (implementation of a cue change) requiring working memory; b) to acquire these strategies and re-use them in same-day subsequent trials T3, T6, and T9 requiring working and short-term memory ability between trials; and c) to remember and implement these strategies



Figure 9. Injection site of α -synuclein pre-formed fibrils.

Following pre-surgery behaviour, mice were administered an injection of PBS or PFFs in the dorsolateral striatum using standardized injection coordinates (+0.5mm AP, +2.1mm ML, and -2.8mm DV). Shown is a brain slice from a mouse that underwent microdialysis probe insertion using the aforementioned stereotaxic coordinates; the needle used for PBS/PFF injections in this experiment is too small to leave a noticeable tract. AP = anteroposterior, DV = dorsoventral, GFAP = glial fibrillary acidic protein, ML = mediolateral, PBS=phosphate buffered saline, PFF=pre-formed fibril.

following a 24h delay in T4 and T7, requiring longer-term memory and intact motivation to perform the task (Figure 12a).

Mice underwent pre-surgery behavioural testing, were administered a unilateral injection of PBS or 5 μ g sonicated PFFs into the right striatum, and were re-tested at 1 and 3 months post-injection. It was not possible to assess injection coordinates by physical damage *post mortem* in these mice; the size of the injection needle was intentionally very small to reduce the potential of tissue damage. However, dye injections and microdialysis probe insertion conducted with the same stereotaxic coordinates and equipment have previously confirmed correct placement of these coordinates within the dorsolateral striatum (Figure 9).

3.2.1 p.G2019S leucine-rich repeat kinase 2 knock-in mice may be more vulnerable to pre-formed fibril-induced motor deficits

Six-month old WT and KI mice underwent cylinder and open field testing immediately prior to injection to establish baseline motor behaviour. WT and KI mice showed comparable

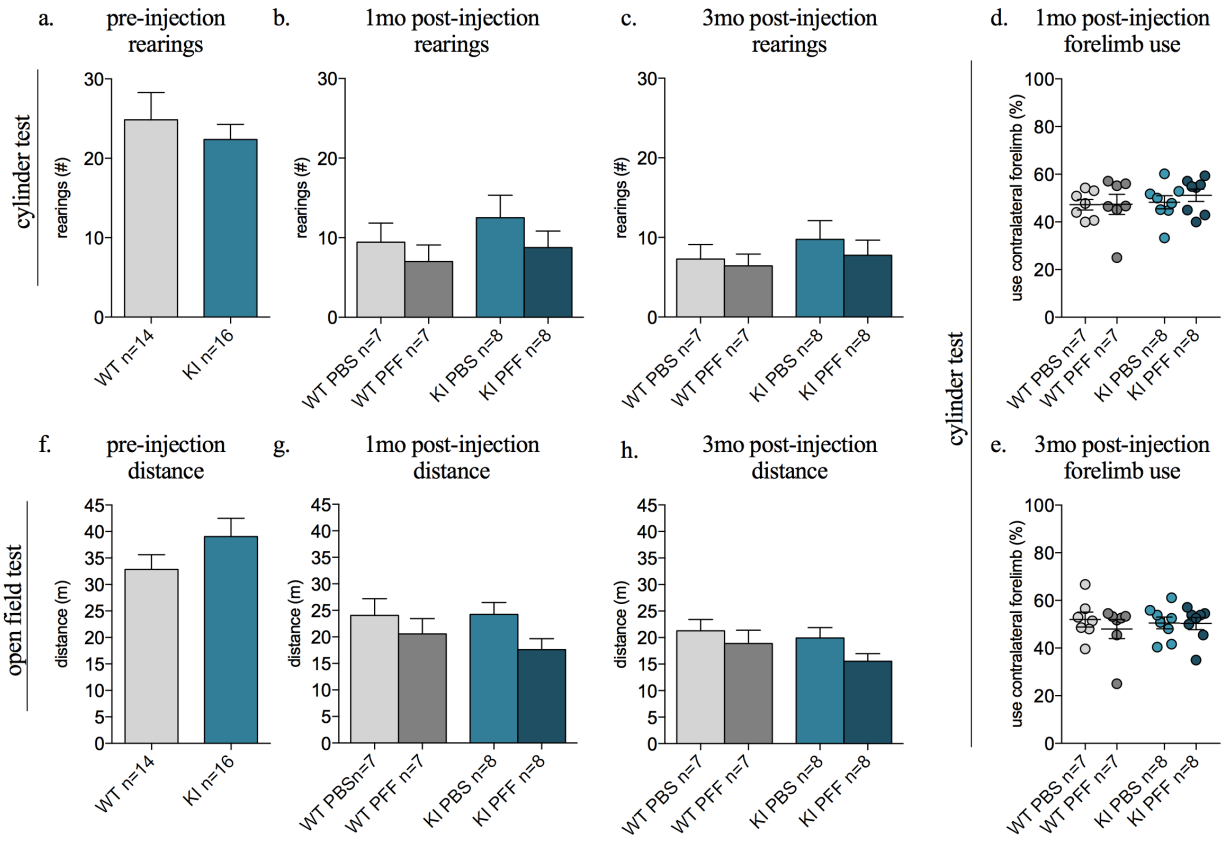


Figure 10. Motor testing of pre-formed fibril-injected lucine-rich repeat kinase 2 p.G2019S knock-in mice. Prior to surgery (six months of age), WT and KI mice demonstrated similar rearing events in the cylinder test (a) and distance travelled in the open field test (f). At both one and three months post-injection, PFF-injected mice of both genotypes trended towards reduced rearing (b, c) but demonstrated no forelimb preference (d, e). Furthermore, at both one and three months post-injection, PFF-injected mice of both genotypes appeared to travel less in the open field (g, h). Forelimb use values are reported as number of wall contacts made with the contralateral forelimb as a percent of the total number of wall contacts made with both forelimbs. Experimental n indicates number of animals. Error bars represent standard errors of the mean. KI=lucine-rich repeat kinase 2 p.G2019S knock-in, m=metres, mo=months, PBS=phosphate-buffered saline, PFF=pre-formed fibril, WT=wild-type.

motor ability as indicated by rearing in the cylinder test (Figure 10a) and distance travelled in the open field arena (Figure 10f). At both one and three months post-injection, all mice exhibited a reduction in general motor activity irrespective of PBS or PFF treatment. This could be due to surgery-induced alterations in performance and/or desensitisation with repeated test exposures. Both WT and KI PFF-injected mice showed similar rearing in the cylinder test relative to PBS-injected controls, and no forelimb preference was observed as might be expected after a unilateral noxious insult (Figure 10d-e). However, a trend towards reduced distance travelled by KI PFF-

injected animals relative to PBS-injected animals in the open field test was noted at both time points (Figure 10g-h). This trend did not reach significance, with 50-60% power at one month post-injection and 30-40% power at three months post-injection. At this stage, these data suggest that KI mice may be more vulnerable to a PFF-induced motor deficit; however, this must be confirmed in future experiments with at least 25 mice per group to achieve 95% power.

3.2.2 p.G2019S leucine-rich repeat kinase 2 knock-in mice are more susceptible to pre-formed fibril-induced anxiety

Baseline anxiety-like behaviours were tested by performance in the cylinder and open field tests in mice prior to injection. WT and KI mice showed similar levels of anxiety as demonstrated by comparable grooming behaviour in the cylinder test (Figure 11a, d) and centre path ratio in the open field test (Figure 10g). At both one and three months post-injection, WT and KI PFF-injected mice showed comparable grooming behaviour relative to PBS-injected mice of the same genotype (Figure 11b-c, e-f). A non-significant trend towards reduced grooming time at three months post-injection in WT PFF-injected was seen ($p=0.15$) (Figure 11f). Of greater interest, PFF-injected KI mice showed a significant reduction in centre path ratio relative to PBS-injected KI mice at one and three months post-injection ($p=0.004, 0.02$), whereas PBS- and PFF-injected WT mice were comparable (Figure 11h, i). Thus, KI mice may be more susceptible to a PFF-induced anxiety phenotype. The power for these data is between 80-85% at one month post-injection and 50-60% at three months post-injection; therefore, the results must be confirmed in future experiments with a sample size of at least 20 mice for 95% power.

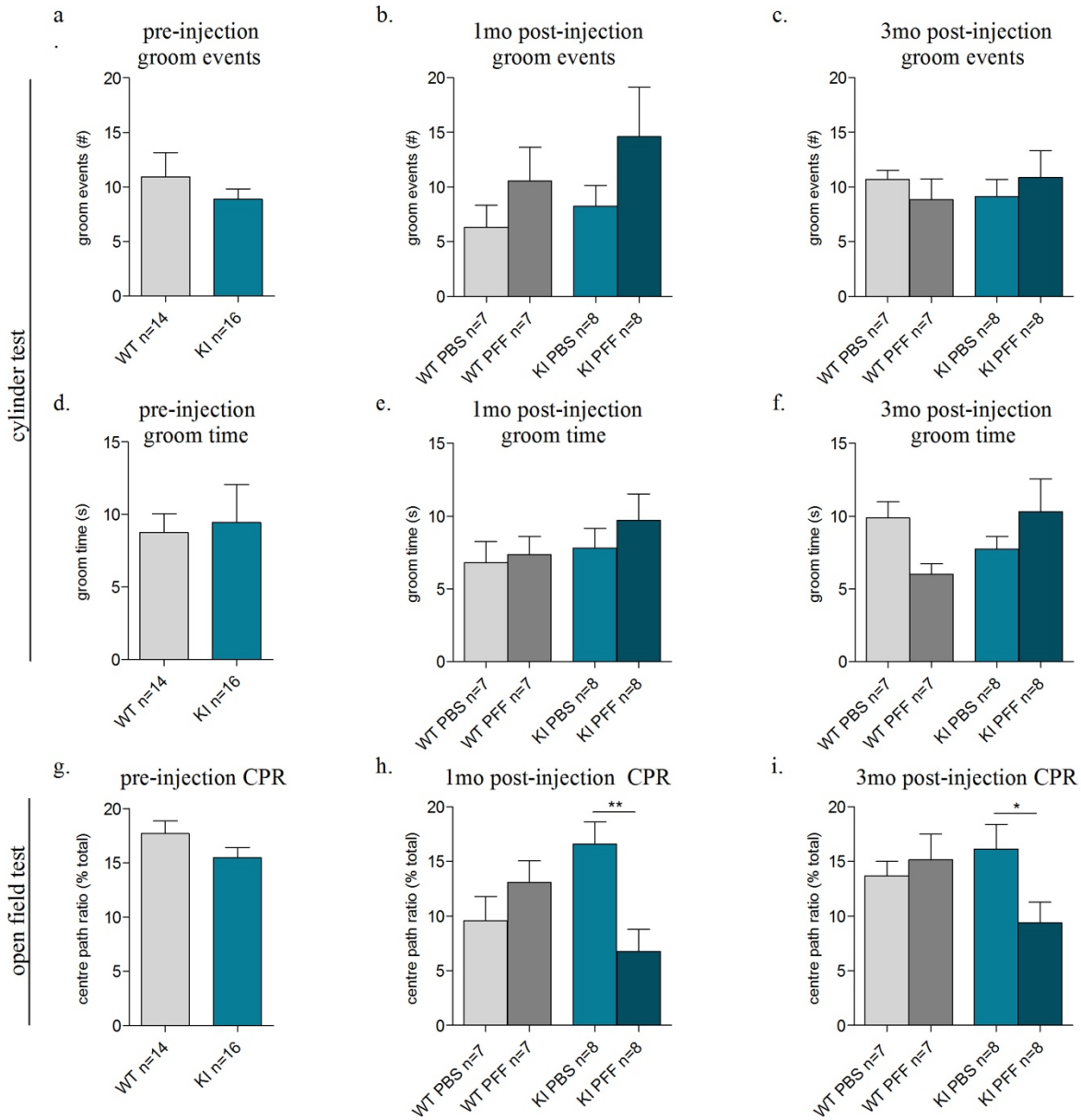


Figure 11. Anxiety testing of pre-formed fibril-injected leucine-rich repeat kinase 2 p.G2019S knock-in mice. Prior to surgery, WT and KI mice demonstrated similar grooming activity in the cylinder test (a, c) and centre path ratio in the open field test (g). At one and three months post-injection, mice from all conditions demonstrated no significant differences in grooming activity (b, c, e, f). However, PFF-injected KI mice demonstrated a significant reduction in centre path ratio at both time points (h, i). Centre path ratio values are reported as distance travelled in the centre area as a percent of total distance travelled. Experimental n indicates number of animals. Error bars represent standard errors of the mean. CPR=centre path ratio, KI=leucine-rich repeat kinase 2 p.G2019S knock-in, m=metres, mo=months, PBS=phosphate-buffered saline, PFF=pre-formed fibril, WT=wild-type. * $p < 0.05$, ** $p < 0.01$ by one-way ANOVA and Bonferroni's post-hoc test.

3.2.3 p.G2019S leucine-rich repeat kinase 2 knock-in mice may be more susceptible to pre-formed fibril-induced cognitive deficits

Performance in the NOL and puzzle box tests was used to assess cognitive ability prior to injection. Whereas WT mice demonstrated learning in NOL with 90-95% power by spending more time with an object moved to a novel location ($p=0.01$), KI mice did not demonstrate the same learning trend (Figure 12a). This observation indicated an intrinsic deficit in spatial recognition and/or memory performance in six month-old KI mice. In contrast, WT and KI mice performed similarly in the puzzle box test, which involves an aversive stimulus and behaviourally relevant goal (Figure 13c).

At one and three months post-injection, WT PBS-injected mice only exhibited a learning trend in the NOL test (Figure 12b, c). This may represent a surgery effect, but is likely due to intrinsic variability in mice and small sample sizes. Indeed, the power for this result is only 20-30% at one month post-injection and 30-40% at three months post-injection. Interestingly, WT PFF-injected mice displayed a clear transient learning deficit in NOL at one month post-injection from which they appeared to recover at three months post-injection (Figure 12b, c). As KI mice were already cognitively impaired prior to surgery, it was expected that both PBS- and PFF-injected KI mice would show deficits at one and three months post-injection (Figure 12b, c). It might be argued that PFF injections induce a cognitive deficit in WT mice similar to the intrinsic deficit observed in six month-old KI animals. PBS- and PFF-injected WT and KI mice performed similarly in all trials of the puzzle box at one month post injection (Figure 13d). However, at three months post-injection, PFF-injected KI mice appeared to be uniquely impaired in trial 6 (repeat of small entry and bedding obstruction) with 60-70% power, in trial 7 (repeat of small entry and bedding obstruction after 24h delay) with 10-20% power, and in trial 9 (repeat of small entry,

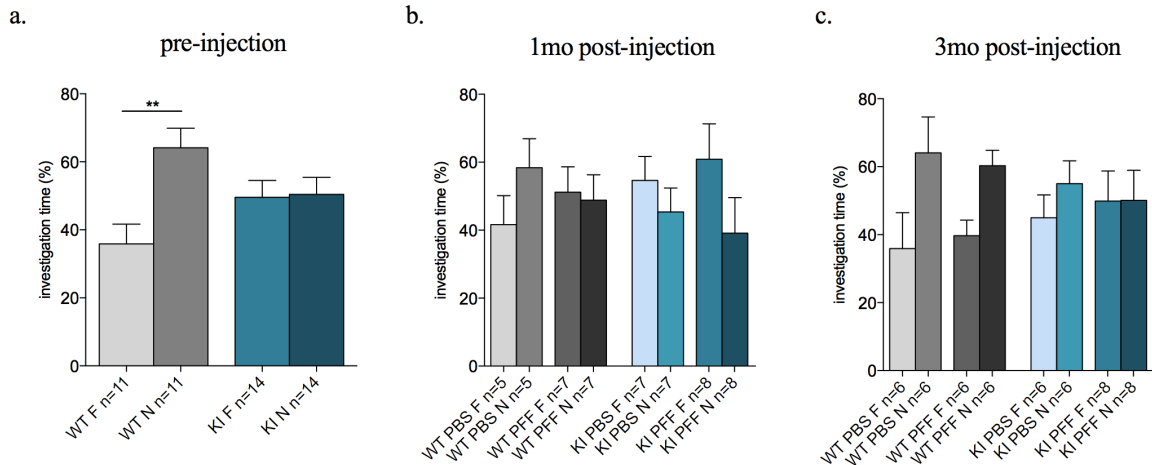


Figure 12. Cognitive testing of pre-formed fibril-injected leucine-rich repeat kinase 2 p.G2019S knock-in mice using the novel object location test.

Prior to surgery, WT mice appeared to be cognitively intact by assessment in the NOL test. However, KI mice appeared to have a cognitive deficit, as they spent a similar amount of time investigating an object moved to a novel location and an object in a familiar location (a). At one month post-injection, PBS-injected WT mice showed a learning trend, but PFF-injected WT mice did not (b). At three months post-injection, PBS-injected WT mice demonstrated significant learning, while PFF-injected WT mice appeared to show a learning trend (c). Similar to pre-injection, KI mice of both conditions did not learn in NOL at one and three months post-injection (b, c). NOL values are reported as time spent investigating each object as a percent of the total time spent investigating both objects. Experimental n indicates number of animals. Error bars represent standard errors of the mean. F=familiar location object, KI=leucine-rich repeat kinase 2 p.G2019S knock-in, mo=months, N=novel location object, PBS=phosphate-buffered saline, PFF=pre-formed fibril, WT=wild-type. **p<0.01 by one-way ANOVA and Bonferroni's post-hoc test.

bedding obstruction, and cue change) with 30-40% power (Figure 13e). Future experiments should include at least 25 animals to elucidate if these results indicate a real effect, but these data suggest a PFF-induced cognitive deficit may exist in KI mice only.

Together, these pilot study data suggest that LRRK2 is involved in neuronal response to induced α -synucleinopathy, and the p.G2019S mutation may exacerbate PFF-induced effects *in vivo*.

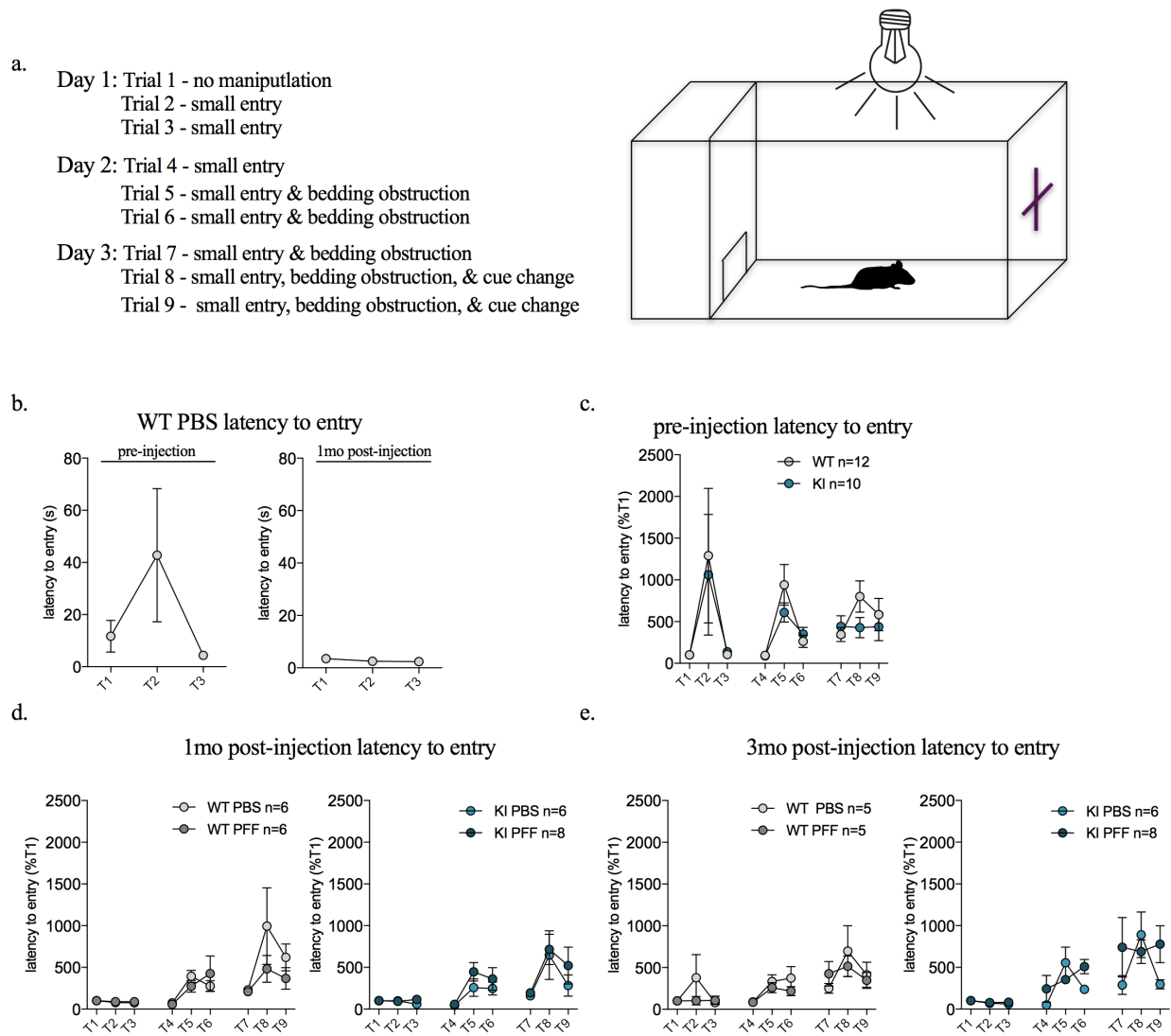


Figure 13. Cognitive testing of pre-formed fibril-injected leucine-rich repeat kinase 2 p.G2019S knock-in mice using the puzzle box test.

Trial conditions are listed in **a**. Comparison between the first round of testing (pre-surgery) and second round of testing (1mo post-surgery) revealed reduced latency to entry with repeated testing (**b**). Prior to surgery, WT and KI mice performed comparably in all trials (**c**). At one month post-injection, PBS- and PFF-injected mice of both genotypes showed similar latencies to entry (**d**). At three months post-injection, WT mice of both treatment conditions performed comparably in all trials (**e**). KI mice of both treatment conditions were similar in most trials, but KI PFF-injected appeared to show increased latency to entry in trials 6 ($p>1$), 7 ($p=0.32$), and 9 ($p=0.23$) (**e**). Latency to entry values are reported as raw values in **b** and as a percent of their initial entry latency in trial 1 in **c-e**. Experimental n indicates number of animals. Error bars represent standard errors of the mean. KI=leucine-rich repeat kinase 2 p.G2019S knock-in, mo=months, PBS=phosphate-buffered saline, PFF=pre-formed fibril, T=trial, WT=wild-type.

4. Discussion

α -Syn and LRRK2 are the most heavily implicated protein candidates in the etiology of PD. Despite this, primary literature examining pathological interactions between these two central proteins is sparse and lacks consensus. Thus, this project aimed to determine whether a) LRRK2 is involved in neuronal and systemic response to induced α -syn pathology, and b) if the p.G2019S mutation alters these responses using optimal models of α -syn aggregation and PD genetic susceptibility. PFFs induce α -syn aggregation that resembles Lewy pathology *in vitro*, and cause diffuse p-syn pathology as well as behavioural phenotypes *in vivo*. As PFF-induced pathogenesis is delayed, progressive, and precedes eventual cell death, this model provides an opportunity to investigate potential disease-modifying therapies. Furthermore, the genetically faithful LRRK2 p.G2019S KI mouse model was used to examine mutant LRRK2 effects on PFF-induced α -syn pathology under endogenous levels and regulation. The KI model avoids confounds of random insertion, underlying endogenous WT expression, and artificial expression patterns.

4.1 Initial characterization of pre-formed fibril treatment

As PFFs were generated in an external facility, TEM was utilized to examine their ultrastructure pre- and post-sonication. The integrity of PFF fibrillar ultrastructure pre-sonication was intact, and the sonication protocol was observed to effectively break up the fibrils into oligomeric seeds as required according to published standardised protocols (Volpicelli-Daley et al., 2014).

Primary cultures were treated with PBS, monomeric α -syn, or sonicated PFFs at DIV7; treatment is recommended following DIV5 as endogenous α -syn is not expressed until this time, and prior to DIV10 as neurons become affected at a much quicker rate in older cultures (Volpicelli-

Daley et al., 2014). Cultures were maintained for 10 days post treatment to allow ample time for seeding and propagation of pathogenic α -syn without inducing excessive toxicity before fixation. While this timeline was suitable for our aims, ongoing experiments are testing whether genotype-dependent vulnerability is maintained, diminished, or exaggerated when treatment occurs in older cells (DIV21-31) or over a longer period (DIV7-22). The 81A anti-p-syn antibody, which is regarded as standard within the field, was used to evaluate induced aggregation of α -syn between PBS- and PFF-treated neurons of both genotypes. To evaluate levels of p-syn staining between genotypes in an unbiased fashion, all p-syn images within a culture were subject to the same thresholding, and mean gray values were normalized to the average field nuclei of their respective conditions to account for cell density differences.

After 10d of treatment, PFF-treated cultures developed punctate and serpentine p-syn-positive aggregates, which appeared to be most numerous in axons and present in ~5% of cell soma. We predict that this is a reflection of pathology propagating from synaptic terminals towards cell bodies; assessment of the number of ACBs over time would be enlightening. As previously observed, we found that the majority of neuritic aggregates were axonal, forming predominantly in MAP2-negative processes (data not shown) (Volpicelli-Daley et al., 2014). To confirm that observed effects were induced by treatment with PFFs specifically and not simply by addition of α -syn, treatment with monomeric α -syn was also performed. Monomeric α -syn did not induce α -synucleinopathy in cultures as indicated by negligible p-syn staining, again confirming previous reports of this model (Volpicelli-Daley et al., 2011).

4.2 The role of leucine-rich repeat kinase 2 in neuronal response to induced α -synucleinopathy by pre-formed fibril treatment

Previously, p.A53T α -syn OE mice that are null for LRRK2 have been reported to show reduced pathology, neurodegeneration, and immune response relative to p.A53T α -syn OE mice with normal LRRK2 expression (Lin et al., 2009). In addition, LRRK2 KO rats and WT rats administered a LRRK2 kinase inhibitor were reported to show protection from virally-expressed α -syn-induced inflammation and nigral degeneration (Daher et al., 2014, 2015). Though promising, these results are limited by use of mutant OE or viral expression of α -syn. Further, aspects of these studies were not replicated when examined by others (Daher et al., 2012; Herzig et al., 2012). To examine the role of LRRK2 in responses to pathogenic α -syn insult using a subtler model of α -synucleinopathy, primary cortical neurons from WT and KO embryos were treated with sonicated PFFs. In a total of five separate cultures, PFF-treated KO neurons displayed significantly reduced p-syn staining relative to PFF-treated WT neurons.

One explanation for this observed reduction may be that LRRK2 neurons are more susceptible to PFF-induced toxicity, but die prior to fixation. To examine this possibility, the LDH-based colorimetric assay was performed using media from each condition at three separate time points over the course of treatment (DIV9, DIV12, and DIV17). At each time point, this assay suggested that PFFs induce a slight reduction in membrane integrity, but no genotypic difference was observed. While useful, the LDH assay is somewhat crude; it is more accurately a measure of cell membrane integrity and media conditions that alter enzymatic activity rather than toxicity *per se*. Therefore, nuclei that were pyknotic, i.e. small, irregular, and containing condensed chromatin (Kroemer et al., 2009), relative to total nuclei in each condition were counted as an additional measure of toxicity. The results supported those of the LDH assay. Together, these data suggest

that the genotypic difference in p-syn staining is not a by-product of increased toxicity in KO cultures; rather, it may indicate a role for LRRK2 in the process of fibril uptake, intracellular handling of fibrils, degradation of pathogenic α -syn, and/or spread of pathogenic α -syn.

To further probe the underlying mechanism of KO protection from PFF-induced α -synucleinopathy, cell bodies that contained pronounced p-syn-positive aggregates (termed affected cell bodies, ACBs) relative to the total number cells were compared between WT and KO neurons. Interestingly, KO neurons displayed a strong trend towards a reduction in the percentage of ACBs relative to WT neurons. However, p-syn staining within ACBs was comparable between WT and KO neurons. These observations suggest that overall p-syn reductions in KO neurons may be due to a) fewer cell bodies being positively stained, and/or b) less p-syn stain in neurites. Indeed, masking out ACBs and re-quantifying mean gray values of p-syn within neurites revealed reduced p-syn staining in neurites. In summary, the cell bodies that succumb to PFF-induced pathogenic effects are equally affected in WT and KO neurons, but fewer KO cell bodies ultimately succumb to these effects, and neurites are less affected. This data suggests that KO protection from PFF treatment may be due to less neurons initially taking up fibrils, more effective degradation of pathogenic α -syn within neurites, or less efficient neuron-to-neuron spread of pathogenic α -syn. These hypotheses should be directly addressed in future experiments.

To investigate potential genotypic differences in markers of autophagy contributing to reduced KO p-syn staining, levels of and p-syn co-localization with p62 and LAMP1 were examined. p62 recognizes and targets toxic intracellular material for autophagy, but the significance of its presence is a subject of current debate. Increased p62 may signify an upregulation of the protein in response to a heightened demand for intracellular degradation; on the other hand, it may indicate a build-up of p62 due to impaired autophagy within the cell (Rusten

and Stenmark, 2010). In contrast, LAMP1 is a transmembrane protein present across lysosomal membranes. We observed that both p62 and LAMP1 tended to predominantly localize to the cell body, which was not surprising given that this is the primary location of protein degradation. Therefore, whole image fields surrounding ACBs were examined in addition to isolated ACBs specifically.

In ACB-containing image fields of three KO cultures, a genotype-independent trend towards increased p62 was observed in PFF-treated neurons relative to PBS-treated neurons, likely reflecting PFF-induced stress on the autophagy pathway. Though others have reported increases in p62 upon LRRK2 inhibition (Manzoni et al., 2013), we observed no significant difference in p62 levels of WT and KO fields or ACBs. Thus, the observed reduction in KO p-syn staining does not appear to correlate with differences in p62 levels. Co-localization with p-syn was quite high in isolated ACBs and relatively less in whole image fields, but no genotypic difference was observed. As KO neurons displayed an overall reduction in total p-syn stain, but similar p-syn and p62 co-localization to WT, KO neurons may be more effective at targeting p-syn for degradation by autophagy with p62.

Interestingly, WT PFF-treated neurons displayed a significant increase in LAMP1 relative to WT PBS-treated neurons, whereas KO PFF-treated neurons only showed a slight, trending increase in LAMP1 relative to KO PBS-treated neurons in two independent cultures. Further, KO PBS-treated neurons showed a very strong trend towards increased LAMP1 relative to WT PBS-treated neurons, whereas WT and KO PFF-treated neurons showed no difference in LAMP1 levels. These data indicate that KO neurons may have intrinsically higher levels of LAMP1, which has been reported in KO kidneys of mice (Tong et al., 2012) and young rats (Baptista et al., 2013). In culture, these neurons may be more prepared to utilise the lysosomal system to effectively deal

with the initial PFF insult. In fact, others have reported that PFFs are immediately surrounded by LAMP1 after neuronal uptake, indicating it is one of the first response mechanisms of the cell to PFF treatment (Tsujimura et al., 2014). As WT neurons appear have intrinsically less LAMP1, they may attempt to respond to PFFs with a strong upregulation of the protein, which might a) not occur swiftly enough to prevent early seeding of endogenous α -syn, and/or b) disrupt homeostasis of degradation pathways and result in less efficient handling of pathogenic α -syn. Alternatively, LRRK2 may promote recycling rather than degradation of vesicle cargoes, reducing both demand for LAMP1-positive lysosomes and degradation of toxic cellular waste. Indeed, silencing LRRK2 has been reported to alter vesicle recycling dynamics, distribution, and motility (Piccoli et al., 2011).

An examination of LAMP1 co-localization with p-syn in ACB-containing fields and isolated ACBs revealed low co-localization that was comparable across genotypes of the same condition. As mentioned, WT and KO cell bodies that ultimately succumb to PFF-treatment appear similarly affected. It is possible that differences in p-syn and LAMP1 co-localization would be seen in regions of the coverslip without ACBs, or if examined at earlier time points before pathogenic α -syn ultimately reaches the cell body. In addition, searching for differences in LAMP1 and p-syn co-localization may be futile; initiation of the degradation process within lysosomes may result in the protein becoming unrecognizable. Indeed, other groups have not observed co-localization with p-syn and LAMP1 (Tanik et al., 2013).

It is important to note that the absence of glial cells was confirmed by absence of staining with anti-Iba1 and anti-GFAP antibodies in primary cortical cultures. Daher et al. have suggested that glial response mediates protection of KO rats from nigral degeneration induced by virally-

expressed α -syn (Daher et al., 2014); however, a purely neuronal protection mechanism is demonstrated by these experiments.

4.3 p.G2019S-induced alterations in neuronal response to induced α -synucleinopathy by pre-formed fibril treatment

Given that LRRK2 appears to play a role in neuronal response to induced α -synucleinopathy by pre-formed fibril treatment, alterations to this response induced by the LRRK2 p.G2019S mutation were examined. Primary cortical neurons from WT and KI embryos were treated with sonicated PFFs in a total of four separate cultures, in which PFF-treated KI neurons displayed significantly elevated p-syn staining relative to PFF-treated WT neurons.

The possibility that differential p-syn staining was a consequence of differences in PFF-induced toxicity was examined solely using condensed nuclei counts given that they were shown to reflect LDH assay results in KO cultures. No differences in the percentage of pyknotic nuclei were observed between treatment conditions or genotypes, suggesting that increased p-syn staining is not a by-product of reduced toxicity in KI cultures. Rather, it may indicate that the p.G2019S mutation influences fibril uptake, intracellular handling of fibrils, degradation of pathogenic α -syn, and/or spread of pathogenic α -syn.

To further probe the mechanism by which KI neurons were more susceptible to PFF-induced α -synucleinopathy, ACBs were compared between WT and KI neurons. The number of ACBs was not different in WT and KI neurons. However, p-syn staining within isolated ACBs was increased in KI neurons relative to WT neurons. Masking out ACBs and re-quantifying mean gray values revealed that p-syn was also increased in KI neurites compared to WT neurites. In summary, these data suggest that fibrils are initially taken up and/or spread from neuron-to-neuron

with similar efficacy in WT and KI neurons, but KI cell bodies and neurites that succumb to PFF-induced pathogenic effects are affected to a greater extent. This data suggests that p.G2019S LRRK2 impairs intracellular handling and/or protein degradation of pathogenic α -syn.

To probe the underlying mechanism of p.G2019S KI vulnerability to PFF treatment, levels of the autophagy marker p62 and its co-localization with p-syn were examined in ACB-containing image fields and isolated ACBs. In ACB-containing image fields from two WT cultures and one KI culture, a non-significant increase in p62 was observed in WT PFF-treated neurons relative to WT PBS-treated neurons, likely reflecting PFF-induced stress on the autophagy pathway (as previously observed in WT and KO neurons). While no significant difference in p62 levels was observed between PBS- and PFF-treated KI neurons, PBS-treated KI neurons appeared to have significantly increased levels of p62 relative to PBS-treated WT neurons. This might indicate an intrinsic increase in the level of this protein in KI neurons, which could be related to a heightened demand for degradation and/or impaired autophagy within the cell. Indeed, others have reported that autophagy is augmented with expression of p.G2019S LRRK2 (Su and Qi, 2013), and p62 specifically has been implicated in p.G2019S-induced increases in depolarization and autophagy of mitochondria (Su et al., 2015). Further, it has been reported that p.G2019S LRRK2 is poorly degraded by chaperone-mediated autophagy (CMA), resulting in compromised integrity of cellular degradation systems (Orenstein et al., 2013).

Furthermore, co-localization of p62 and p-syn was significantly higher in KI than WT neurons. Although increased p-syn staining in PFF-treated KI neurons may have contributed to this observation, p62 levels were not different between PFF-treated neurons of either genotype, suggesting that increased co-localization is not simply a consequence of increased protein levels. This provides further evidence towards intrinsically impaired degradation processes in KI neurons

that may increase susceptibility to pathogenic α -syn insult. While p-syn and p62 co-localization was significantly higher in KI image fields relative to WT, it was not in KI ACBs relative to WT. This may indicate that p62 is effectively targeting p-syn in KI neurites specifically, but impaired autophagy is preventing its degradation.

It is important to note that while vulnerability of p.G2019S KI neurons to PFF treatment could be the result a direct relationship between LRRK2 and α -syn, it may also be due to non-specific susceptibility to insult conferred by the mutation. Assays testing susceptibility to other inducible insults such as glutamate excitotoxicity should be pursued to examine this possibility. However, if p.G2019S KI neurons are generally more vulnerable, this would not negate the importance of an increased susceptibility to PD-like pathological processes; indeed, it has been suggested for many years that PD may be a form of accelerated aging (Kish et al., 1992) to which mutant-induced neuronal vulnerability might generally contribute.

4.4 p.G2019S-induced alterations in behavioural deficits caused by intrastriatal pre-formed fibril injection

Given that a) intracerebral PFF injection has been previously reported to induce motor deficits in WT mice (Luk et al., 2012a), and b) KI neurons were more vulnerable to PFF-treatment *in vitro*, behavioural consequences of PFF injection in WT and KI mice were compared to examine if the p.G2019S mutation conferred increased susceptibility to PFFs *in vivo* in a pilot study. To holistically characterize the behaviour of WT and KI mice pre-and post-injection, performance was examined in the cylinder, open field, NOL, and puzzle box tests. The same array of behavioural tests was performed at one and three months post-injection to examine potential genotypic differences PFF-induced behavioural alterations, and results were evaluated in the

context of pre-injection behaviour. Motor ability was determined by rearing in the cylinder test and distance traveled in the open field test. Anxiety behaviours were observed in the cylinder test by grooming activity and the open field test by centre path ratio (i.e. percentage of total distance travelled that was in the centre area). Cognitive ability was tested in the NOL and puzzle box spatial-based learning tests. NOL results were reported as percentage of time investigating an object in a novel location relative to one in a familiar location, and puzzle box results were reported as either raw latency to entry or as a percentage of T1 latency to chamber to account for intrinsic motivation of each mouse to enter the dark chamber.

Baseline behavioural differences in six-month-old WT and KI mice were examined prior to injection. Our own group has observed no difference between WT and KI mice in motor and anxiety behaviours at this age (unpublished data). This was reflected in the results of pre-surgery testing, which showed no motor differences between WT and KI mice in cylinder and open field testing. However, previously unreported differences in cognitive performance emerged. Mice typically prefer novelty, and will spend more time investigating an object in a novel location relative to one in a familiar location after initial object exposure; this forms the basis of the NOL test. While six month-old WT mice demonstrated ‘learning’ in this testing paradigm by spending more time with an object in a novel location relative to one in a familiar location, KI mice showed a cognitive deficit. Given that LRRK2 and the p.G2019S mutation alter synaptic function *in vitro* and in the striatum (Beccano-Kelly et al., 2014; Yue et al., 2015), a multi-input integrative structure that influences habitual, goal-directed and spatiotemporal behaviours (Jahanshahi et al., 2015), this cognitive deficit is predictable. However, in the puzzle box paradigm, which presents mice with a more aversive test that has a behaviourally relevant end-point (i.e. dark chamber entry to avoid bright light and potential threat), WT and KI mice were comparable in performance.

Intrastriatal injection of PFFs in WT mice induces motor deficits in the wire hang test at three months post-injection and in the rotarod test at six months post-injection, which paralleled observed α -syn pathology in motor behaviour-related regions of the brain (Luk et al., 2012a). In the experiments here, PFF-injected WT and KI mice showed similar rearing in the cylinder test when compared to PBS-injected mice at one and three months post-injection. Neither PBS- nor PFF-injected mice demonstrated a preference for the ipsilateral forelimb at either time point, suggesting there was no PFF-induced deficit specific to the contralateral forelimb. In the open field test, KI PFF-injected mice demonstrated a trend to reduced distance traveled at both time points relative to PBS-injected mice, but the small sample size of this demi-cohort prevented this trend from reaching significance. These results suggest KI mice may be more susceptible to PFF-induced motor deficits, but this hypothesis must be tested in future large-scale experiments with at least 25 animals per condition.

No groups have reported anxiety or cognitive phenotypes in PFF-injected mice as of yet. At one and three months post-injection, PBS- and PFF-injected mice of both genotypes exhibited normal behaviour in cylinder test grooming activity. PFF-injected WT mice did not display alterations to centre path ratio in the open field test relative to PBS-injected WT mice; however, KI mice displayed a significant reduction in centre path ratio at both time points with relatively high power. These data indicate a genotype-specific PFF-induced anxiety phenotype that should be confirmed by future experiments. While the mechanistic underpinnings of this phenotype are likely complicated, it is worth noting that anxiety is a known pre-clinical, non-motor symptom in PD patients (Berg et al., 2015).

With regards to cognitive behavioural assessments, it should be noted that PBS-injected WT control mice did not significantly discriminate between objects in a familiar vs. novel location

post-injection in the NOL test, though a learning trend existed with low power. Though this could represent a surgery-induced effect, it is likely due to small sample size and would conceivably become significant with future large-scale testing. Interestingly, a clear but transient NOL deficit in WT PFF-injected mice emerged at one month post-injection and disappeared at three months post-injection. This could be a surgery effect, or it may be a PFF-induced disruption in cognitive ability that is overcome with compensatory learning strategies acquired over time. PBS- and PFF-injected KI mice did not display learning at any time point in the NOL test, consistent with observed performance of these mice pre-surgery.

Performance on all trials of the puzzle box test appeared similar in PBS- and PFF-injected mice of both genotypes at one month post-injection. However, by three months post injection, PFF-injected KI mice uniquely displayed an increased latency to entry on strategy acquisition and memory trials. While PFF-injected KI mice appear capable of finding the dark chamber entrance when the task becomes more challenging, they appear less capable of acquiring and remembering the strategy necessary to do so in subsequent trials. As previously discussed, the striatum is a multi-input integration structure that affects goal-directed behaviours (Jahanshahi et al., 2015). The presence of the p.G2019S LRRK2 mutation alone has been reported to induce striatal synaptic dysfunction (Beccano-Kelly et al., 2014, 2015); thus, it is conceivable that an additional intrastriatal PFF insult would exacerbate any basal deficit and perhaps impair the goal-directed spatiotemporal function required to enter the dark chamber. Whether a genotype-specific treatment effect truly exists must be elucidated in future experiments with at least 25 animals per condition.

4.5 Limitations and future directions

4.5.1 Markers of α -synucleinopathy *in vitro*

As previously noted, the use of the 81A anti-p-syn antibody as a marker of aggregated α -syn is somewhat standard in the field, but not without controversy as it has been observed to non-specifically bind neurofilament (Sacino et al., 2014). In agreement with Sacino et al., we observed some non-specific staining primarily in white matter tracts. Consistently, the occasional axon was observed to be p-syn-positive in PBS-treated *in vitro* conditions. However, this staining was much dimmer than presumed α -syn aggregate staining, and was mostly eliminated by equal thresholding applied to all images. Therefore, it may be reasonable to assume that antibody non-specificity did not significantly influence the results of these experiments. Though the 81A antibody was utilized in these experiments for the sake of consistency with both the field and previously conducted experiments in the lab, replication using a more specific antibody has been conducted (ab59264) and very similar results obtained (data not shown).

4.5.2 Mechanisms of genotypic differences *in vitro*

While the underlying mechanisms of KO protection and KI susceptibility were examined to an extent in the experiments presented here, additional cultures as well as protein analyses should be added to solidify observed trends. In addition, the hypotheses outlined regarding underlying mechanisms of genotypic differences should be tested in future experiments. Though differences in LAMP1 levels were observed in KO cultures, LAMP1 was not examined in KI cultures due to unforeseen technical issues. This is obviously lacking in this set of experiments and should be examined.

4.5.3 Immunohistochemistry staining *in vivo*

Unfortunately, due to the longitudinal nature of behavioural characterization experiments, confirmation of pathology in PFF-injected mice has yet to be observed. A small subset of mice from these experiments were perfused, and analysis of PFF-induced pathology is ongoing. As PFF-induced pathology has been repeatedly observed by others (Luk et al., 2012a, 2012b; Sacino et al., 2014; Paumier et al., 2015; Peelaerts et al., 2015), and our protocol did not substantively differ from these other groups, we expect to observe p-syn staining.

5. Conclusion

Taken together, these experiments implicate LRRK2 and the p.G2019S mutation in multiple aspects of α -syn pathogenic processes. *In vitro*, knocking out LRRK2 results in protection from PFF-induced α -synucleinopathy. This is apparently due to reduced initial uptake of PFFs, more effective degradation of pathogenic α -syn in neurites, or less efficient neuron-to-neuron spread of pathogenic α -syn. In contrast, the LRRK2 p.G2019S mutation increases susceptibility to PFF treatment, likely due to impaired handling or degradation of pathogenic α -syn. Following a unilateral intrastriatal PFF injection, onset of PFF-induced motor deficits appears to be accelerated in KI mice. Furthermore, PFF-injected KI mice display unique anxiety and cognitive deficits, potentially reflecting increased susceptibility to striatal synaptic deficits. Further experiments are required to confirm observed trends and to elucidate mechanisms underlying genotypic differences, but these initial findings prove promising in their contribution to the field's understanding of LRRK2 in α -synuclein pathobiology.

Bibliography

- Anandhan A, Rodriguez-Rocha H, Bohovych I, Griggs AM, Zavala-Flores L, Reyes-Reyes EM, Seravalli J, Stanciu LA, Lee J, Rochet JC, Khalimonchuk O, Franco R (2015) Overexpression of α -synuclein at non-toxic levels increases dopaminergic cell death induced by copper exposure via modulation of protein degradation pathways. *Neurobiol Dis* 81:76–92 Available at: <http://dx.doi.org/10.1016/j.nbd.2014.11.018>.
- Arnold SE, Toledo JB, Appleby DH, Xie SX, Wang L-S, Baek Y, Wolk DA, Lee EB, Miller BL, Lee VM-Y, Trojanowski JQ (2013) Comparative survey of the topographical distribution of signature molecular lesions in major neurodegenerative diseases. *J Comp Neurol* 521:4339–4355 Available at: <http://www.ncbi.nlm.nih.gov/pubmed/23881776> [Accessed April 18, 2016].
- Baptista MAS, Dave KD, Frasier MA, Sherer TB, Greeley M, Beck MJ, Varsho JS, Parker GA, Moore C, Churchill MJ, Meshul CK, Fiske BK (2013) Loss of leucine-rich repeat kinase 2 (LRRK2) in rats leads to progressive abnormal phenotypes in peripheral organs. *PLoS One* 8:1–16.
- Bartels T, Choi JG, Selkoe DJ (2011) α -Synuclein occurs physiologically as a helically folded tetramer that resists aggregation. *Nature* 477:107–110 Available at: <http://dx.doi.org/10.1038/nature10324>.
- Beccano-Kelly DA, Kuhlmann N, Tatarnikov I, Volta M, Munsie LN, Chou P, Cao L-P, Han H, Tapia L, Farrer MJ, Milnerwood AJ (2014) Synaptic function is modulated by LRRK2 and glutamate release is increased in cortical neurons of G2019S LRRK2 knock-in mice. *Front Cell Neurosci* 8:301 Available at: <http://journal.frontiersin.org/article/10.3389/fncel.2014.00301/abstract>.

- Beccano-Kelly DA, Volta M, Lise LN, Paschall SA, Tatarnikov I, Co K, Chou P, Cao LP, Bergeron S, Mitchell E, Han H, Melrose HL, Tapia L, Raymond LA, Matthew MJ, Milnerwood AJ (2015) LRRK2 overexpression alters glutamatergic presynaptic plasticity, striatal dopamine tone, postsynaptic signal transduction, motor activity and memory. *Hum Mol Genet* 24:1336–1349.
- Berg D et al. (2015) MDS research criteria for prodromal Parkinson's disease. *Mov Disord* 30:1600–1611.
- Bjorkoy G, Lamark T, Brech A, Outzen H, Perander M, ??vervatn A, Stenmark H, Johansen T (2005) p62/SQSTM1 forms protein aggregates degraded by autophagy and has a protective effect on huntingtin-induced cell death. *J Cell Biol* 171:603–614.
- Braak H, Tredici K Del, Rüb U, de Vos RA., Jansen Steur EN., Braak E (2003) Staging of brain pathology related to sporadic Parkinson's disease. *Neurobiol Aging* 24:197–211.
- Burke RE, Dauer WT, Vonsattel JPG (2008) A critical evaluation of the Braak staging scheme for Parkinson's disease. *Ann Neurol* 64:485–491.
- Burré J, Sharma M, Tsetsenis T, Buchman V, Etherton MR, Südhof TC (2010) α -Synuclein Promotes SNARE-Complex Assembly in vivo and in vitro. *Science* (80-) 329:1663–1667.
- Carballo-Carbajal I, Weber-Endress S, Rovelli G, Chan D, Wolozin B, Klein CL, Patenge N, Gasser T, Kahle PJ (2010) Leucine-rich repeat kinase 2 induces α -synuclein expression via the extracellular signal-regulated kinase pathway. *Cell Signal* 22:821–827 Available at: <http://dx.doi.org/10.1016/j.cellsig.2010.01.006>.
- Chesselet M-F, Richter F (2011) Modelling of Parkinson's disease in mice. *Lancet Neurol* 10:1108–1118 Available at: <http://linkinghub.elsevier.com/retrieve/pii/S1474442211702277>.

- Clark LN, Wang Y, Karlins E, Saito L, Mejia-Santana H, Harris J, Louis ED, Cote LJ, Andrews H, Fahn S, Waters C, Ford B, Frucht S, Ottman R, Marder K (2006) Frequency of LRRK2 mutations in early- and late-onset Parkinson disease. *Neurology* 67:1786–1791.
- Conway K a, Lee SJ, Rochet JC, Ding TT, Williamson RE, Lansbury PT (2000) Acceleration of oligomerization, not fibrillization, is a shared property of both α -synuclein mutations linked to early-onset Parkinson's disease: implications for pathogenesis and therapy. *Proc Natl Acad Sci U S A* 97:571–576.
- Dachsel JC, Behrouz B, Yue M, Beevers JE, Melrose HL, Farrer MJ (2010) A comparative study of LRRK2 function in primary neuronal cultures. *Park Relat Disord* 16:650–655 Available at: <http://dx.doi.org/10.1016/j.parkreldis.2010.08.018>.
- Daher JPL, Abdelmotilib HA, Hu X, Volpicelli-Daley LA, Moehle MS, Faser KB, Needle E, Chen Y, Steyn SJ, Galatsis P, Hirst WD, West AB (2015) LRRK2 pharmacological inhibition abates α -synuclein induced neurodegeneration. *J Biol Chem* 290:19433–19444 Available at: <http://www.jbc.org/content/290/32/19433.full>.
- Daher JPL, Pletnikova O, Biskup S, Musso A, Gellhaar S, Galter D, Troncoso JC, Lee MK, Dawson TM, Dawson VL, Moore DJ (2012) Neurodegenerative phenotypes in an A53T α -synuclein transgenic mouse model are independent of LRRK2. *Hum Mol Genet* 21:2420–2431.
- Daher JPL, Volpicelli-Daley LA, Blackburn JP, Moehle MS, West AB (2014) Abrogation of α -synuclein-mediated dopaminergic neurodegeneration in LRRK2-deficient rats. *Proc Natl Acad Sci U S A* 111:9289–9294 Available at: <http://www.pnas.org/content/111/25/9289>.
- Danzer KM, Haasen D, Karow AR, Moussaud S, Habeck M, Giese A, Kretschmar H, Hengerer B, Kostka M (2007) Different species of α -synuclein oligomers induce calcium influx and

seeding. *J Neurosci* 27:9220–9232.

Davies P, Hinkle KM, Sukar NN, Sepulveda B, Mesias R, Serrano G, Alessi DR, Beach TG, Benson DL, White CL, Cowell RM, Das SS, West AB, Melrose HL (2013) Comprehensive characterization and optimization of anti-LRRK2 (leucine-rich repeat kinase 2) monoclonal antibodies. *Biochem J* 453:101–113 Available at: <http://www.pubmedcentral.nih.gov/articlerender.fcgi?artid=3682752&tool=pmcentrez&rendertype=abstract>.

Desplats P, Lee H-J, Bae E-J, Patrick C, Rockenstein E, Crews L, Spencer B, Masliah E, Lee S-J (2009) Inclusion formation and neuronal cell death through neuron-to-neuron transmission of α -synuclein. *Proc Natl Acad Sci U S A* 106:13010–13015 Available at: <http://www.pnas.org/content/106/31/13010.long>.

Dickson DW (2012) Parkinson's disease and parkinsonism: Neuropathology. *Cold Spring Harb Perspect Med* 2 Available at: <http://www.ncbi.nlm.nih.gov/pubmed/22908195> [Accessed April 18, 2016].

Dickson DW, Uchikado H, Fujishiro HF, Tsuboi Y (2010) Evidence in favor of Braak staging of Parkinson's disease. *Mov Disord* 25:78–82.

Emmanouilidou E, Stefanis L, Vekrellis K (2010) Cell-produced α -synuclein oligomers are targeted to, and impair, the 26S proteasome. *Neurobiol Aging* 31:953–968 Available at: <http://dx.doi.org/10.1016/j.neurobiolaging.2008.07.008>.

Fredenburg RA, Rospigliosi C, Meray RK, Kessler JC, Lashuel HA, Eliezer D, Lansbury PT (2007) The impact of the E46K mutation on the properties of α -synuclein in its monomelic and oligomeric states. *Biochemistry* 46:7107–7118.

Freundt EC, Maynard N, Clancy EK, Roy S, Bousset L, Sourigues Y, Covert M, Melki R,

- Kirkegaard K, Brahic M (2012) Neuron-to-neuron transmission of α -synuclein fibrils through axonal transport. *Ann Neurol* 72:517–524 Available at: <http://doi.wiley.com/10.1002/ana.23747> [Accessed April 18, 2016].
- Fuchs J, Nilsson C, Kachergus J, Munz M, Larsson E-M, Schule B, Langston JW, Middleton FA, Ross OA, Hulihan M, Gasser T, Farrer MJ (2007) Phenotypic variation in a large Swedish pedigree due to SNCA duplication and triplication. *Neurology* 68:916–922 Available at: <http://www.neurology.org/cgi/doi/10.1212/01.wnl.0000254458.17630.c5> [Accessed April 19, 2016].
- Fujiwara H, Hasegawa M, Dohmae N, Kawashima A, Masliah E, Goldberg MS, Shen J, Takio K, Iwatsubo T (2002) α -Synuclein is phosphorylated in synucleinopathy lesions. *Nat Cell Biol* 4:160–164 Available at: <http://www.nature.com/ncb/journal/v4/n2/abs/ncb748.html>.
- Garcia-Reitböck P, Anichtchik O, Bellucci A, Iovino M, Ballini C, Fineberg E, Ghetti B, Della Corte L, Spano P, Tofaris GK, Goedert M, Spillantini MG (2010) SNARE protein redistribution and synaptic failure in a transgenic mouse model of Parkinson's disease. *Brain* 133:2032–2044.
- Gosavi N, Lee HJ, Lee JS, Patel S, Lee SJ (2002) Golgi fragmentation occurs in the cells with prefibrillar α -synuclein aggregates and precedes the formation of fibrillar inclusion. *J Biol Chem* 277:48984–48992.
- Guerreiro PS, Huang Y, Gysbers A, Cheng D, Gai WP, Outeiro TF, Halliday GM (2013) LRRK2 interactions with α -synuclein in Parkinson's disease brains and in cell models. *J Mol Med* 91:513–522.
- Häbig K, Gellhaar S, Heim B, Djuric V, Giesert F, Wurst W, Walter C, Hentrich T, Riess O, Bonin M (2013) LRRK2 guides the actin cytoskeleton at growth cones together with

ARHGEF7 and Tropomyosin 4. *Biochim Biophys Acta - Mol Basis Dis* 1832:2352–2367

Available at: <http://dx.doi.org/10.1016/j.bbadis.2013.09.009>.

Hentati F, Trinh J, Thompson C, Nosova E, Farrer MJ, Aasly JO (2014) LRRK2 parkinsonism in Tunisia and Norway: A comparative analysis of disease penetrance. *Neurology* 83:568–569.

Herzig MC, Bidinosti M, Schweizer T, Hafner T, Stemmelen C, Weiss A, Danner S, Vidotto N, Stauffer D, Barske C, Mayer F, Schmid P, Rovelli G, van der Putten PH, Shimshek DR (2012) High LRRK2 levels fail to induce or exacerbate neuronal alpha-synucleinopathy in mouse brain. *PLoS One* 7.

Irwin DJ, Lee VM-YM-Y, Trojanowski JQ (2013) Parkinson's disease dementia: convergence of α -synuclein, tau and amyloid- β pathologies. *Nat Rev Neurosci* 14:626–636 Available at: <http://www.pubmedcentral.nih.gov/articlerender.fcgi?artid=4017235&tool=pmcentrez&rendertype=abstract> \n<http://www.nature.com/doifinder/10.1038/nrn3549>.

Jahanshahi M, Obeso I, Rothwell JC, Obeso JA (2015) A fronto–striato–subthalamic–pallidal network for goal-directed and habitual inhibition. *Nat Rev Neurosci* 16:719–732 Available at: <http://www.nature.com/doifinder/10.1038/nrn4038> [Accessed June 8, 2016].

Kachergus J, Mata IF, Hulihan M, Taylor JP, Lincoln S, Aasly J, Gibson JM, Ross OA, Lynch T, Wiley J, Payami H, Nutt J, Maraganore DM, Czyzewski K, Styczynska M, Wszolek ZK, Farrer MJ, Toft M (2005) Identification of a novel LRRK2 mutation linked to autosomal dominant parkinsonism: evidence of a common founder across European populations. *Am J Hum Genet* 76:672–680 Available at: <http://www.pubmedcentral.nih.gov/articlerender.fcgi?artid=1199304&tool=pmcentrez&rendertype=abstract>.

Karpinar DP et al. (2009) Pre-fibrillar α -synuclein variants with impaired beta-structure increase

- neurotoxicity in Parkinson's disease models. *Eur Mol Biol Organ J* 28:3256–3268.
- Kirik D, Rosenblad C, Burger C, Lundberg C, Johansen TE, Muzyczka N, Mandel RJ, Björklund A (2002) Parkinson-like neurodegeneration induced by targeted overexpression of α -synuclein in the nigrostriatal system. *J Neurosci* 22:2780–2791.
- Kish SJ, Shannak K, Rajput A, Deck JH, Hornykiewicz O (1992) Aging produces a specific pattern of striatal dopamine loss: implications for the etiology of idiopathic Parkinson's disease. *J Neurochem* 58:642–648 Available at:
<http://www.ncbi.nlm.nih.gov/pubmed/1729408>
<http://onlinelibrary.wiley.com/store/10.1111/1/j.1471-4159.1992.tb09766.x/asset/j.1471-4159.1992.tb09766.x.pdf?v=1&t=i9tqap2o&s=48ea6d4f1d05f647086e955b40e2d54bc761b356>
<http://www.ncbi.nlm.nih.gov/pubmed/1729408>.
- Koprich JB, Johnston TH, Huot P, Reyes MG, Espinosa M, Brotchie JM (2011) Progressive neurodegeneration or endogenous compensation in an animal model of Parkinson's disease produced by decreasing doses of α -synuclein. *PLoS One* 6:1–9.
- Kordower JH, Chu Y, Hauser R a, Freeman TB, Olanow CW (2008) Lewy body-like pathology in long-term embryonic nigral transplants in Parkinson's disease. *Nat Med* 14:504–506.
- Kroemer G et al. (2009) Classification of cell death: Recommendations of the Nomenclature Committee on Cell Death 2009. *Cell Death Differ* 16:3–11 Available at:
<http://www.ncbi.nlm.nih.gov/pmc/articles/PMC2744427/>.
- Leveridge M, Collier L, Edge C, Hardwicke P, Leavens B, Ratcliffe S, Rees M, Stasi LP, Nadin A, Reith AD (2016) A high-throughput screen to identify LRRK2 kinase inhibitors for the treatment of Parkinson's disease using RapidFire mass spectrometry. *J Biomol Screen* 21:145–155.

- Li X, Patel JC, Wang J, Avshalumov M V, Nicholson C, Buxbaum JD, Elder GA, Rice ME, Yue Z (2010) Enhanced striatal dopamine transmission and motor performance with LRRK2 overexpression in mice is eliminated by familial Parkinson's disease mutation G2019S. *J Neurosci Off J Soc Neurosci* 30:1788–1797 Available at: <http://www.jneurosci.org/content/30/5/1788.full>.
- Lin C-H, Tsai P-I, Wu R-M, Chien C-T (2010) LRRK2 G2019S mutation induces dendrite degeneration through mislocalization and phosphorylation of tau by recruiting autoactivated GSK3 β . *J Neurosci Off J Soc Neurosci* 30:13138–13149 Available at: <http://www.ncbi.nlm.nih.gov/pubmed/20881132>.
- Lin MK, Farrer MJ (2014) Genetics and genomics of Parkinson's disease. *Genome Med* 6:1–16.
- Lin X, Parisiadou L, Gu XL, Wang L, Shim H, Sun L, Xie C, Long CX, Yang WJ, Ding J, Chen ZZ, Gallant PE, Tao-Cheng JH, Rudow G, Troncoso JC, Liu Z, Li Z, Cai H (2009) Leucine-rich repeat kinase 2 regulates the progression of neuropathology induced by Parkinson's-disease-related mutant α -synuclein. *Neuron* 64:807–827 Available at: <http://dx.doi.org/10.1016/j.neuron.2009.11.006>.
- Lo Bianco C, Ridet J-L, Schneider BL, Deglon N, Aebischer P (2002) α -Synucleinopathy and selective dopaminergic neuron loss in a rat lentiviral-based model of Parkinson's disease. *Proc Natl Acad Sci U S A* 99:10813–10818 Available at: <http://www.pubmedcentral.nih.gov/articlerender.fcgi?artid=125054&tool=pmcentrez&rendertype=abstract>.
- Longo F, Russo I, Shimshek DR, Greggio E, Morari M (2014) Genetic and pharmacological evidence that G2019S LRRK2 confers a hyperkinetic phenotype, resistant to motor decline associated with aging. *Neurobiol Dis* 71:62–73 Available at:

<http://dx.doi.org/10.1016/j.nbd.2014.07.013>.

Luk KC et al. (2012a) Pathological α -synuclein transmission initiates Parkinson-like neurodegeneration in nontransgenic mice. *Science* (80-) 338:949–953 Available at: <http://www.ncbi.nlm.nih.gov/pubmed/23161999> [Accessed April 18, 2016].

Luk KC, Kehm VM, Zhang B, O'Brien P, Trojanowski JQ, Lee VMY (2012b) Intracerebral inoculation of pathological α -synuclein initiates a rapidly progressive neurodegenerative α -synucleinopathy in mice. *J Exp Med* 209:975–986 Available at: <http://jem.rupress.org/content/209/5/975.long>.

MacLeod D, Dowman J, Hammond R, Leete T, Inoue K, Abeliovich A (2006) The familial parkinsonism gene LRRK2 regulates neurite process morphology. *Neuron* 52:587–593.

Manzoni C, Mamais A, Dihanich S, Abeti R, Soutar MPM, Plun-Favreau H, Giunti P, Tooze SA, Bandopadhyay R, Lewis PA (2013) Inhibition of LRRK2 kinase activity stimulates macroautophagy. *Biochim Biophys Acta - Mol Cell Res* 1833:2900–2910 Available at: <http://dx.doi.org/10.1016/j.bbamcr.2013.07.020>.

Martinez-Vicente M, Vila M (2013) Alpha-synuclein and protein degradation pathways in Parkinson's disease: A pathological feed-back loop. *Exp Neurol* 247:308–313 Available at: <http://dx.doi.org/10.1016/j.expneurol.2013.03.005>.

Mazzulli JR, Mishizen AJ, Giasson BI, Lynch DR, Thomas SA, Nakashima A, Nagatsu T, Ota A, Ischiropoulos H (2006) Cytosolic catechols inhibit α -synuclein aggregation and facilitate the formation of intracellular soluble oligomeric intermediates. *J Neurosci* 26:10068–10078 Available at: <http://www.jneurosci.org/cgi/doi/10.1523/JNEUROSCI.0896-06.2006>.

Melrose HL et al. (2010) Impaired dopaminergic neurotransmission and microtubule-associated protein tau alterations in human LRRK2 transgenic mice. *Neurobiol Dis* 40:503–517.

- Miller DW, Hague SM, Clarimon J, Baptista M, Gwinn-Hardy K, Cookson MR, Singleton AB (2004) α -Synuclein in blood and brain from familial Parkinson disease with SNCA locus triplication. *Neurology* 62:1835–1838.
- Mosharov E V., Larsen KE, Kanter E, Phillips KA, Wilson K, Schmitz Y, Krantz DE, Kobayashi K, Edwards RH, Sulzer D (2009) Interplay between cytosolic dopamine, calcium, and α -synuclein causes selective death of substantia nigra neurons. *Neuron* 62:218–229 Available at: <http://dx.doi.org/10.1016/j.neuron.2009.01.033>.
- Nalls M a et al. (2014) Large-scale meta-analysis of genome-wide association data identifies six new risk loci for Parkinson's disease. *Nat Genet* 56:1–7 Available at: <http://www.nature.com/doi/10.1038/ng.3043> <http://www.ncbi.nlm.nih.gov/pubmed/25064009>.
- Nemani VM, Lu W, Berge V, Nakamura K, Onoa B, Lee MK, Chaudhry FA, Nicoll RA, Edwards RH (2010) Increased expression of α -synuclein reduces neurotransmitter release by inhibiting synaptic vesicle reclustering after endocytosis. *Neuron* 65:66–79 Available at: <http://dx.doi.org/10.1016/j.neuron.2009.12.023>.
- Nishioka K, Ross OA, Ishii K, Kachergus JM, Ishiwata K, Kitagawa M, Kono S, Obi T, Mizoguchi K, Inoue Y, Imai H, Takanashi M, Mizuno Y, Farrer MJ, Hattori N (2009) Expanding the clinical phenotype of SNCA duplication carriers. *Mov Disord* 24:1811–1819 Available at: <http://doi.wiley.com/10.1002/mds.22682> [Accessed April 27, 2016].
- Olanow CW, Prusiner SB (2009) Is Parkinson's disease a prion disorder? *Proc Natl Acad Sci U S A* 106:12571–12572.
- Orenstein SJ, Kuo S, Tasset I, Arias E, Koga H, Fernandez-Carasa I (2013) Interplay of LRRK2 with chaperone-mediated autophagy. *Nat Neurosci* 16:394-.

- Ozelius LJ, Senthil G, Saunders-Pullman R, Ohmann E, Deligtisch A, Tagliati M, Hunt AL, Klein C, Henick B, Hailpern SM, Lipton RB, Soto-Valencia J, Risch N, Bressman SB (2006) LRRK2 G2019S as a cause of Parkinson's disease in Ashkenazi Jews. *N Engl J Med* 354:424–425.
- Paisán-Ruíz C et al. (2004) Cloning of the gene containing mutations that cause PARK8-linked Parkinson's disease. *Neuron* 44:595–600 Available at: <http://www.ncbi.nlm.nih.gov/pubmed/15541308>.
- Pankiv S, Clausen TH, Lamark T, Brech A, Bruun JA, Outzen H, Øvervatn A, Bjørkøy G, Johansen T (2007) p62/SQSTM1 binds directly to Atg8/LC3 to facilitate degradation of ubiquitinated protein aggregates by autophagy. *J Biol Chem* 282:24131–24145.
- Parisiadou L, Xie C, Cho HJ, Lin X, Gu X-L, Long C-X, Lobbestael E, Baekelandt V, Taymans J-M, Sun L, Cai H (2009) Phosphorylation of ezrin/radixin/moesin proteins by LRRK2 promotes the rearrangement of actin cytoskeleton in neuronal morphogenesis. *J Neurosci Off J Soc Neurosci* 29:13971–13980 Available at: <http://www.pubmedcentral.nih.gov/articlerender.fcgi?artid=2807632&tool=pmcentrez&rendertype=abstract>.
- Parkinson J (1817) *An essay on the shaking palsy*. Whittingham Rowl.
- Parkkinen L, Kauppinen T, Pirttilä T, Autere JM, Alafuzoff I (2005) α -Synuclein pathology does not predict extrapyramidal symptoms or dementia. *Ann Neurol* 57:82–91.
- Paumier KL, Luk KC, Manfredsson FP, Kanaan NM, Lipton JW, Collier TJ, Steece-Collier K, Kemp CJ, Celano S, Schulz E, Sandoval IM, Fleming S, Dirr E, Polinski NK, Trojanowski JQ, Lee VM, Sortwell CE (2015) Intrastriatal injection of pre-formed mouse α -synuclein fibrils into rats triggers α -synuclein pathology and bilateral nigrostriatal degeneration.

Neurobiol Dis 82:185–199.

Paxinos G, Franklin KBJ (2004) *The Mouse Brain in Stereotaxic Coordinates*, 2nd ed. Houston: Gulf Professional Publishing.

Peelaerts W, Bousset L, Van der Perren A, Moskalyuk A, Pulizzi R, Giugliano M, Van den Haute C, Melki R, Baekelandt V (2015) α -Synuclein strains cause distinct synucleinopathies after local and systemic administration. *Nature* 522:340–344 Available at: <http://www.ncbi.nlm.nih.gov/pubmed/26061766>.

Piccoli G, Condliffe SB, Bauer M, Giesert F, Boldt K, De Astis S, Meixner A, Sarioglu H, Vogt-Weisenhorn DM, Wurst W, Gloeckner CJ, Matteoli M, Sala C, Ueffing M (2011) LRRK2 controls synaptic vesicle storage and mobilization within the recycling pool. *J Neurosci* 31:2225–2237 Available at: <http://www.jneurosci.org/cgi/doi/10.1523/JNEUROSCI.3730-10.2011>.

Polymeropoulos MH, Lavedan C, Leroy E, et al. (1997) Mutation in the α -synuclein gene identified in families with Parkinson's disease. *Science* (80-) 276:2045 Available at: <http://jnnp.bmj.com/cgi/doi/10.1136/jnnp.2003.021873> [Accessed April 18, 2016].

Pringsheim T, Jette N, Frolkis A, Steeves TDL (2014) The prevalence of Parkinson's disease: A systematic review and meta-analysis. *Mov Disord* 29:1583–1590 Available at: <http://doi.wiley.com/10.1002/mds.25945> [Accessed April 18, 2016].

Qing H, Wong W, McGeer EG, McGeer PL (2009) Lrrk2 phosphorylates alpha synuclein at serine 129: Parkinson disease implications. *Biochem Biophys Res Commun* 387:149–152 Available at: <http://dx.doi.org/10.1016/j.bbrc.2009.06.142>.

Rajput A, Dickson DW, Robinson CA, Ross OA, D??chsel JC, Lincoln SJ, Cobb SA, Rajput ML, Farrer MJ (2006) Parkinsonism, Lrrk2 G2019S, and tau neuropathology. *Neurology*

67:1506–1508.

Ross OA, Toft M, Whittle AJ, Johnson JL, Papapetropoulos S, Mash DC, Litvan I, Gordon MF, Wszolek ZK, Farrer MJ, Dickson DW (2006) Lrrk2 and Lewy body disease. *Ann Neurol* 59:388–393.

Rusten TE, Stenmark H (2010) p62, an autophagy hero or culprit? *Nat Cell Biol* 12:207–209
Available at: <http://dx.doi.org/10.1038/ncb0310-207>.

Sacino AN, Brooks M, Thomas MA, McKinney AB, McGarvey NH, Rutherford NJ, Ceballos-Diaz C, Robertson J, Golde TE, Giasson BI (2014) Amyloidogenic α -synuclein seeds do not invariably induce rapid, widespread pathology in mice. *Acta Neuropathol* 127:645–665
Available at: <http://link.springer.com/10.1007/s00401-014-1268-0> [Accessed April 18, 2016].

Sacino AN, Thomas M a, Ceballos-Diaz C, Cruz PE, Rosario AM, Lewis J, Giasson BI, Golde TE (2013) Conformational templating of α -synuclein aggregates in neuronal-glia cultures. *Mol Neurodegener* 8:17 Available at:
<http://www.pubmedcentral.nih.gov/articlerender.fcgi?artid=3671973&tool=pmcentrez&rendertype=abstract>.

Schreij AM, Chaineau M, Ruan W, Lin S, Barker P a, Fon E a, McPherson PS (2015) LRRK2 localizes to endosomes and interacts with clathrin-light chains to limit Rac1 activation. *EMBO Rep* 16:79–86 Available at: <http://www.ncbi.nlm.nih.gov/pubmed/25427558>.

Schwab AJ, Ebert AD (2015) Neurite aggregation and calcium dysfunction in iPSC-derived sensory neurons with Parkinson's disease-related LRRK2 G2019S mutation. *Stem Cell Reports* 5:1039–1052 Available at: <http://dx.doi.org/10.1016/j.stemcr.2015.11.004>.

Singleton AB, Farrer M, Johnson J, Singleton A, S. H, J. K (2003) α -synuclein locus triplication

causes Parkinson's disease. *Science* (80-):841 Available at:

<http://go.galegroup.com.ezproxy.library.ubc.ca/ps/i.do?p=HRCA&u=ubcolumbia&id=GAL>

[E|A110621596&v=2.1&it=r&sid=summon&userGroup=ubcolumbia&authCount=1](http://go.galegroup.com.ezproxy.library.ubc.ca/ps/i.do?p=HRCA&u=ubcolumbia&id=GAL)

[Accessed April 19, 2016].

Sloan M, Alegre-Abarrategui J, Potgieter D, Kaufmann A-K, Exley R, Deltheil T, Threlfell S, Connor-Robson N, Brimblecombe K, Wallings R, Cioroch M, Bannerman DM, Bolam JP, Magill PJ, Cragg SJ, Dodson PD, Wade-Martins R (2016) LRRK2 BAC transgenic rats develop progressive, L-DOPA-responsive motor impairment, and deficits in dopamine circuit function. *Hum Mol Genet* 25:951–963 Available at:

<http://www.pubmedcentral.nih.gov/articlerender.fcgi?artid=4754049&tool=pmcentrez&rendertype=abstract>.

Sloan M, Alegre-Abarrategui J, Wade-Martins R (2012) Insights into LRRK2 function and dysfunction from transgenic and knockout rodent models. *Biochem Soc Trans* 40:1080–1085 Available at: <http://www.ncbi.nlm.nih.gov/pubmed/22988869> [Accessed June 5, 2016].

Smith Y, Wichmann T, Factor SA, DeLong MR (2012) Parkinson's disease therapeutics: New developments and challenges since the introduction of levodopa.

Neuropsychopharmacology 37:213–246 Available at:

<http://www.ncbi.nlm.nih.gov/pubmed/21956442> [Accessed April 18, 2016].

Steger M, Tonelli F, Ito G, Davies P, Trost M, Vetter M, Wachter S, Lorentzen E, Duddy G, Wilson S, Baptista MA, Fiske BK, Fell MJ, Morrow JA, Reith AD, Alessi DR, Mann M (2016) Phosphoproteomics reveals that Parkinson's disease kinase LRRK2 regulates a subset of Rab GTPases. *Elife* 5:1–28.

- Stern MB, Lang A, Poewe W (2012) Toward a redefinition of Parkinson's disease. *Mov Disord* 27:54–60 Available at: <http://doi.wiley.com/10.1002/mds.24051> [Accessed April 18, 2016].
- Su YC, Guo X, Qi X (2015) Threonine56 phosphorylation of Bcl-2 is required for LRRK2 G2019S-induced mitochondrial depolarization and autophagy. *Biochem Biophys Acta* 1852:12–21.
- Su YC, Qi X (2013) Inhibition of excessive mitochondrial fission reduced aberrant autophagy and neuronal damage caused by LRRK2 G2019S mutation. *Hum Mol Genet* 22:4545–4561.
- Südhof TC, Rizo J, Su TC, Südhof TC, Rizo J (2011) Synaptic vesicle exocytosis. *Cold Spring Harb Perspect Biol* 3:1–14 Available at: <http://www.ncbi.nlm.nih.gov/pubmed/22026965>.
- Tanik SA, Schultheiss CE, Volpicelli-Daley LA, Brunden KR, Lee VMY (2013) Lewy body-like α -synuclein aggregates resist degradation and impair macroautophagy. *J Biol Chem* 288:15194–15210 Available at: <http://www.ncbi.nlm.nih.gov/pubmed/23532841> [Accessed April 18, 2016].
- Tong Y, Giaime E, Yamaguchi H, Ichimura T, Liu Y, Si H, Cai H, Bonventre J V, Shen J (2012) Loss of leucine-rich repeat kinase 2 causes age-dependent bi-phasic alterations of the autophagy pathway. *Mol Neurodegener* 7:2 Available at: <http://www.molecularneurodegeneration.com/content/7/1/2>.
- Trinh J, Farrer MJ (2013) Advances in the genetics of Parkinson disease.pdf. *Nat Rev Neurol* 9:445–454.
- Tsujimura A, Taguchi K, Watanabe Y, Tatebe H, Tokuda T, Mizuno T, Tanaka M (2014) Lysosomal enzyme cathepsin B enhances the aggregate forming activity of exogenous α -synuclein fibrils. *Neurobiol Dis* 73:244–253.
- Volles MJ, Lansbury PT (2002) Vesicle permeabilization by protofibrillar α -synuclein is

sensitive to Parkinson's disease-linked mutations and occurs by a pore-like mechanism. *Biochemistry* 41:4595–4602.

Volpicelli-Daley LA, Abdelmotilib H, Liu Z, Stoyka L, Daher JPL, Milnerwood AJ, Unni VK, Hirst WD, Yue Z, Zhao HT, Fraser K, Kennedy RE, West AB (2016a) G2019S-LRRK2 expression augments α -synuclein sequestration into inclusions in neurons. *J Neurosci* 36:7415–7427.

Volpicelli-Daley LA, Kirik D, Stoyka LE, Standaert DG, Harms AS (2016b) How can rAAV- α -synuclein and the fibril α -synuclein models advance our understanding of Parkinson disease? *J Neurochem*:n/a-n/a Available at: <http://doi.wiley.com/10.1111/jnc.13627>.

Volpicelli-Daley LA, Luk KC, Lee VM-Y (2014) Addition of exogenous α -synuclein preformed fibrils to primary neuronal cultures to seed recruitment of endogenous α -synuclein to Lewy body and Lewy neurite-like aggregates. *Nat Protoc* 9:2135–2146 Available at: <http://www.pubmedcentral.nih.gov/articlerender.fcgi?artid=4372899&tool=pmcentrez&rendertype=abstract>.

Volpicelli-Daley LA, Luk KC, Patel TP, Tanik S a, Riddle DM, Stieber A, Meany DF, Trojanowski JQ, Lee VM (2011) Exogenous α -synuclein fibrils induce Lewy body pathology leading to synaptic dysfunction and neuron death. *Neuron* 72:57–71.

Volta M, Cataldi S, Beccano-Kelly D, Munsie L, Tatarnikov I, Chou P, Bergeron S, Mitchell E, Lim R, Khinda J, Lloret A, Bennett CF, Paradiso C, Morari M, Farrer MJ, Milnerwood AJ (2015a) Chronic and acute LRRK2 silencing has no long-term behavioral effects, whereas wild-type and mutant LRRK2 overexpression induce motor and cognitive deficits and altered regulation of dopamine release. *Park Relat Disord* 21:1156–1163 Available at: <http://dx.doi.org/10.1016/j.parkreldis.2015.07.025>.

- Volta M, Milnerwood AJ, Farrer MJ (2015b) Insights from late-onset familial parkinsonism on the pathogenesis of idiopathic Parkinson's disease. *Lancet Neurol Pers View* 14:1054–1064.
- Welchko RM, Lévêque XT, Dunbar GL (2012) Genetic rat models of Parkinson's disease. *Parkinsons Dis* 2012.
- West AB, Moore DJ, Biskup S, Bugayenko A, Smith WW, Ross C a, Dawson VL, Dawson TM (2005) Parkinson's disease-associated mutations in leucine-rich repeat kinase 2 augment kinase activity. *Proc Natl Acad Sci U S A* 102:16842–16847 Available at: <http://www.pnas.org/content/102/46/16842.full.pdf>.
- Westphal CH, Chandra SS (2013) Monomeric synucleins generate membrane curvature. *J Biol Chem* 288:1829.
- Winner B, Jappelli R, Maji SK, Desplats PA, Boyer L (2011) In vivo demonstration that α -synuclein oligomers are toxic. *Proc Natl Acad Sci* 108:4194–4199 Available at: <http://www.pnas.org/content/108/10/4194.short>.
- Wood SJ, Wypych J, Steavenson S, Louis J, Citron M, Biere AL (1999) α -Synuclein fibrillogenesis is nucleation-dependent. *J Biol Chem* 274:19509–19513.
- Xilouri M, Vogiatzi T, Vekrellis K, Park D, Stefanis L (2009) Abberant α -synuclein confers toxicity to neurons in part through inhibition of chaperone-mediated autophagy. *PLoS One* 4:16–20.
- Xu Q, Shenoy S, Li C (2012) Mouse models for LRRK2 Parkinson's disease. *Parkinsonism Relat Disord* 18:S186–S189 Available at: [http://dx.doi.org/10.1016/S1353-8020\(11\)70058-X](http://dx.doi.org/10.1016/S1353-8020(11)70058-X).
- Yamada M, Iwatsubo T, Mizuno Y, Mochizuki H (2004) Overexpression of α -synuclein in rat substantia nigra results in loss of dopaminergic neurons, phosphorylation of α -synuclein and

activation of caspase-9: Resemblance to pathogenetic changes in Parkinson's disease. *J Neurochem* 91:451–461.

Yue M et al. (2015) Progressive dopaminergic alterations and mitochondrial abnormalities in LRRK2 G2019S knock-in mice. *Neurobiol Dis* 78:172–195 Available at:
<http://dx.doi.org/10.1016/j.nbd.2015.02.031>.

Zimprich A et al. (2004) Mutations in LRRK2 cause autosomal-dominant parkinsonism with pleomorphic pathology. *Neuron* 44:601–607.